Atlantic Meridional Overturning Circulation - atmospheric pCO_2 feedback in a hosing simulation in the Community Earth System Model v2

Amber Boot[1], Anna S. von der Heydt[1,2], and Henk A. Dijkstra[1,2]

[1]Institute for Marine and Atmospheric research Utrecht, Department of Physics, Utrecht University, Utrecht, the Netherlands
[2]Center for Complex Systems Studies, Utrecht University, Utrecht, the Netherlands

Correspondence: A. Boot <d.boot@uu.nl>

Abstract. The Atlantic Meridional Overturning Circulation (AMOC) is thought to be a tipping element in the Earth System with multiple stable states. Currently, the AMOC is in a state of strong overturning, but studies have shown that climate change might tip the AMOC to a state of weak overturning. Changing the state of the AMOC affects the global climate, and especially the climate in the North Atlantic. Due to disrupted meridional heat transport, the Northern Hemisphere is expected to cool while the Southern Hemisphere is expected to warm. Besides effects on the climate, the AMOC also influences the carbon cycle by transporting important tracers such as nutrients and Dissolved Inorganic Carbon. Deep water formation in the North Atlantic is, for example, an important pathway of carbon from the surface to the deep ocean. It can therefore be expected that a weakening of the AMOC affects the marine carbon cycle and therefore also atmospheric pCO_2. Here, we investigate the effect of a forced AMOC weakening on the marine carbon cycle and atmospheric pCO_2 using simulations performed with the Community Earth System Model v2 (CESM2). We force the simulations with the emission driven SSP1-2.6 and SSP5-8.5 scenario and additionally, force the simulations with an additional freshwater flux in the North Atlantic Ocean. This so-called hosing weakens the AMOC on top of a weakening caused by the greenhouse gas emissions. We use these simulations to determine how much and through what mechanisms, an AMOC weakening affects the air-sea gas exchange of CO_2.

1 Introduction

Anthropogenic emissions of greenhouse gases cause our Earth System to change and warm up. The Earth System is comprised of several subsystems driven by nonlinear dynamics and feedbacks. An important component of the Earth System is the ocean since it acts as a large heat and carbon reservoir and is the most important component on multidecadal to millennial timescales. In the ocean, the Atlantic Meridional Overturning Circulation (AMOC) is an important circulation pattern which shapes the global, and specifically, the North Atlantic climate (Vellinga and Wood, 2008; Palter, 2015). Studies suggest the AMOC has shown large variability in past climates and is related to large climatic events during the glacial-interglacial cycles (e.g. Heinrich events; Rahmstorf, 2002; Lynch-Stieflitz, 2017). Under anthropogenic forcing, the AMOC is expected to reduce in strength in the future (Weijer et al., 2020), and it has been suggested that the AMOC has already been decreasing over the past 50 years

(Dima and Lohmann, 2010). A decrease in the AMOC strength could have a large impact on the North Atlantic and global climate in the future.

Since the AMOC transports heat northward, a weakening in the AMOC strenght effects local temperatures. Generally, an AMOC weakening is associated with decreasing surface air temperature (SATs) and sea surface tmeperatrures (SSTs) in the North Atlantic, accompanied with a small warming of the Southern Hemisphere. This pattern of cooling in the Northern Hemisphere and warming in the Southern Hemisphere is often called the bipolar seesaw effect (Rahmstorf, 2002). Furthermore, a weakening of the AMOC has also been related to changes in the water cycle (Vellinga and Wood, 2002; Jackson et al., 2015). Through teleconnections, a weakening of the AMOC is also associated with changes in the Indian Monsoon and the El Nino - Southern Oscillation (ENSO) phenomenon (Liu et al., 2023).

The changes of the AMOC to the climate system result in changes in the carbon cycle on both the land and in the ocean. As the AMOC is an important current system, it advects tracers important for the carbon cycle such as nutrients which fuel primary production and Dissolved Inorganic Carbon (DIC). Through changes in the carbon cycle, the AMOC influences atmospheric pCO_2, and therefore influences SATs and the water cycle (Weijer et al., 2019; Barker and Knorr, 2021), which in turn can influence the wind and buoyancy forcing of the AMOC. From this we can see that there is a carbon cycle - climate feedback loop associated with the strength of the AMOC. In Gottschalk et al. (2019) it was shown that the response of atmospheric pCO_2 to an AMOC weakening is dependent on the used model, climatic boundary conditions and timescales assessed. Generally, most studies show an increase in atmospheric pCO_2 following an AMOC weakening (e.g. Marchal et al., 1998; Schmittner and Galbraith, 2008; Matsumoto and Yokoyama, 2013), but there is a wide spread in the mechanisms controlling this response. Some studies point to the terrestrial biosphere as the dominant reservoir, while others point to the ocean.

In this study, we investigate the AMOC - atmospheric pCO_2 feedback, which is a complex, nonlinear feedback and a potential source of uncertainty for future projections. We therefore aim to improve the understanding of the AMOC - atmospheric pCO_2 relation following an AMOC weakening, and answer the following question: what is the effect of a forced AMOC weakening on atmospheric pCO_2?

2 Method

For this study we use simulations of the Community Earth System Model v2 (CESM2; Danabasoglu et al., 2020) simulated on the Dutch supercomuputer (Snellius). CESM2 is a fully coupled model including atmospheric dynamics (CAM6), land processes (CLM5), sea ice processes (CICE5), and ocean circulation (POP2; Smith et al., 2010) and biogeochemistry (MARBL; Long et al., 2021). Both POP2 and MARBL are run on a displaced Greenland pole grid at a nominal horizontal resolution of 1°, with 60 non-equidistant vertical levels. In MARBL, several elemental cycles, three explicit phytoplankton functional groups (small phytoplankton, diatoms, and diazotrophs), one implicit phytoplankton group (calcifiers), and one zooplankton group are simulated.

We analyze simulations forced by greenhouse gas emissison following the Shared Socioeconomic Pathway (SSP) scenarios SSP1-2.6 and SSP5-8.5 (O'Neill et al., 2020). Emission driven simulations are used to be able to study the feedbacks between

the ocean and atmosphere carbon reservoirs. For both scenarios we have a control simulation with just the greenhouse gas emissions, and what we call 'hosing' simulations. In the hosing simulations, the model is additionally forced with a freshwater flux at a rate of 0.5 Sv in the North Atlantic Ocean. The freshwater flux will perturb the density structure of the ocean which will lead to a AMOC weakening.

All simulations are initialized from a emissions driven historical simulation performed by NCAR as part of the Coupled Model Intercomparison Project 6 (CMIP6; Eyring et al., 2016). The simulations shown here run from 2015 to 2100, and the analysis is based on monthly averaged data. Line plots are smoothed with a 5 year moving mean. The control simulations are denoted with CTL, and the hosing simulations with HOS; the SSP scenarios are differentiated on their number (i.e. 126 and 585). We therefore have 4 runs we name CTL-126, HOS-126, CTL-585 and HOS-585.

3 Results

Below I present some additional results corresponding to the material in the presentation. The CTL-585 and HOS-585 simulations are for the period 2015-2100, and CTL-126 and HOS-126 for the period 2015-2050 (by time of writing this document the simulations were up to 2050; I will update the figures once the simulation is finished).

List of figures:

1. AMOC streamfunction SSP5-8.5
2. AMOC strength SSP5-8.5
3. GMST SSP5-8.5
4. Surface Air Temperature SSP5-8.5
5. Sea Surface Temperature SSP5-8.5
6. Sea Surface Salinity SSP5-8.5
7. Precipitation minus evaporation SSP5-8.5
8. Air-sea gas exchange SSP5-8.5
9. Net Biosphere Production SSP5-8.5
10. CO_2 concentration SSP5-8.5
11. Air-sea and air-land exchange of CO_2 SSP5-8.5
12. Net Primary Production SSP5-8.5
13. Export Production SSP5-8.5

14. Surface pH SSP5-8.5

15. Ocean CO_2 uptake per basin SSP5-8.5

16. Variables in the Arctic SSP5-8.5

17. Variables in the Pacific SSP5-8.5

18. Variables in the Pacific SSP5-8.5

19. Variables in the Atlantic SSP5-8.5

20. AMOC streamfunction SSP1-2.6

21. AMOC strength SSP1-2.6

22. GMST SSP1-2.6

23. Surface Air Temperature SSP1-2.6

24. Sea Surface Temperature SSP1-2.6

25. Sea Surface Salinity SSP1-2.6

26. Precipitation minus evaporation SSP1-2.6

27. Air-sea gas exchange SSP1-2.6

28. Net Biosphere Production SSP1-2.6

29. CO_2 concentration SSP1-2.6

30. Air-sea and air-land exchange of CO_2 SSP1-2.6

31. Net Primary Production SSP1-2.6

32. Export Production SSP1-2.6

33. Surface pH SSP1-2.6

34. Ocean CO_2 uptake per basin SSP1-2.6

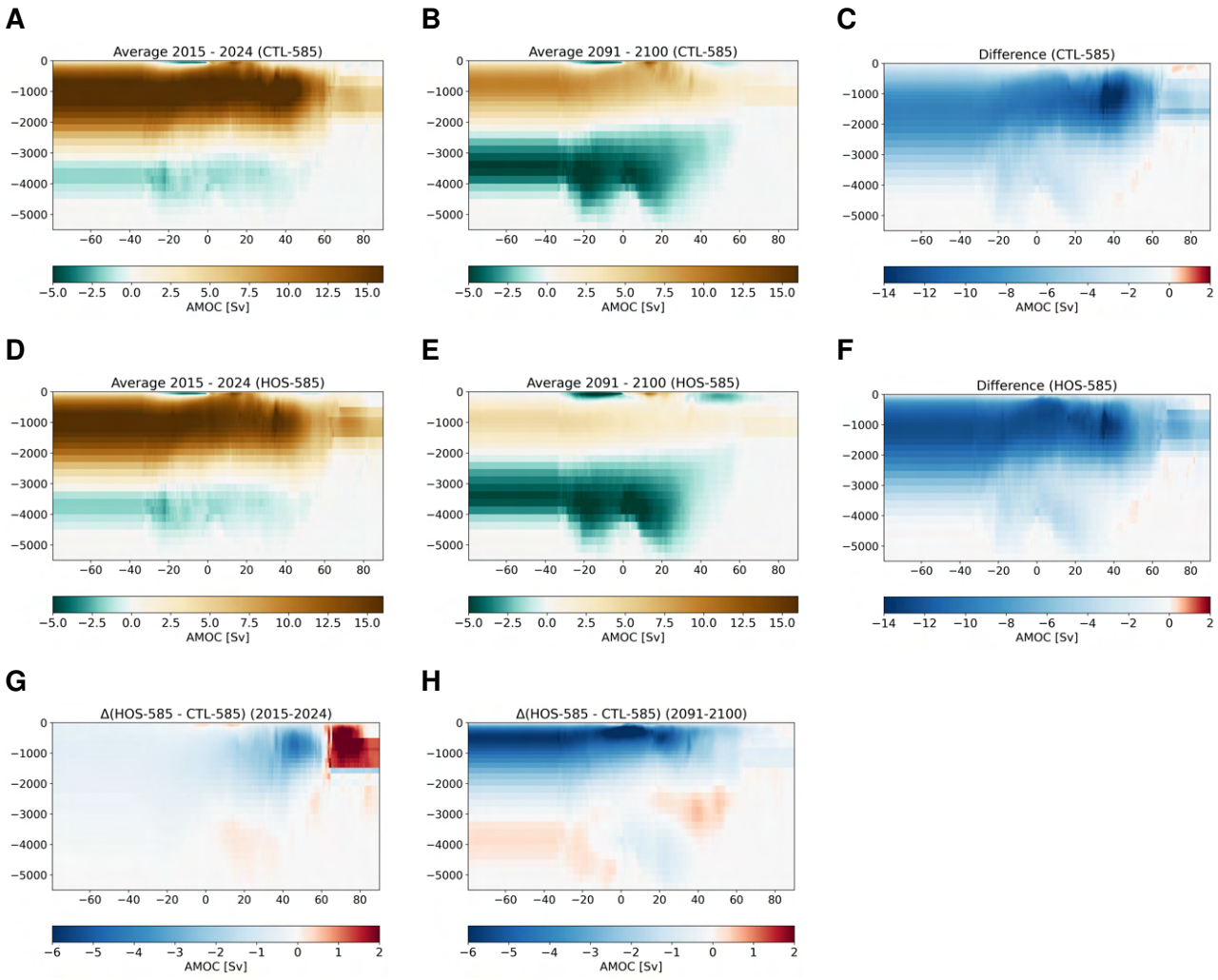

Figure 1. Atlantic Meridional Overturning Circulation streamfunction in Sverdrup (10^6 m^3 s^{-1}) for CTL-585 and HOS-585 and the difference between the two. The top row represents CTL-585 (A-C), the middle row HOS-585 (D-F), and the bottom row the difference (HOS-585 minus CTL-585; G, H). The left column represents the first decade (2015-2024; A, D, G), the middle column the last decade (2091-2100; B, E, H), and the right column the difference (last minus first; C, F).

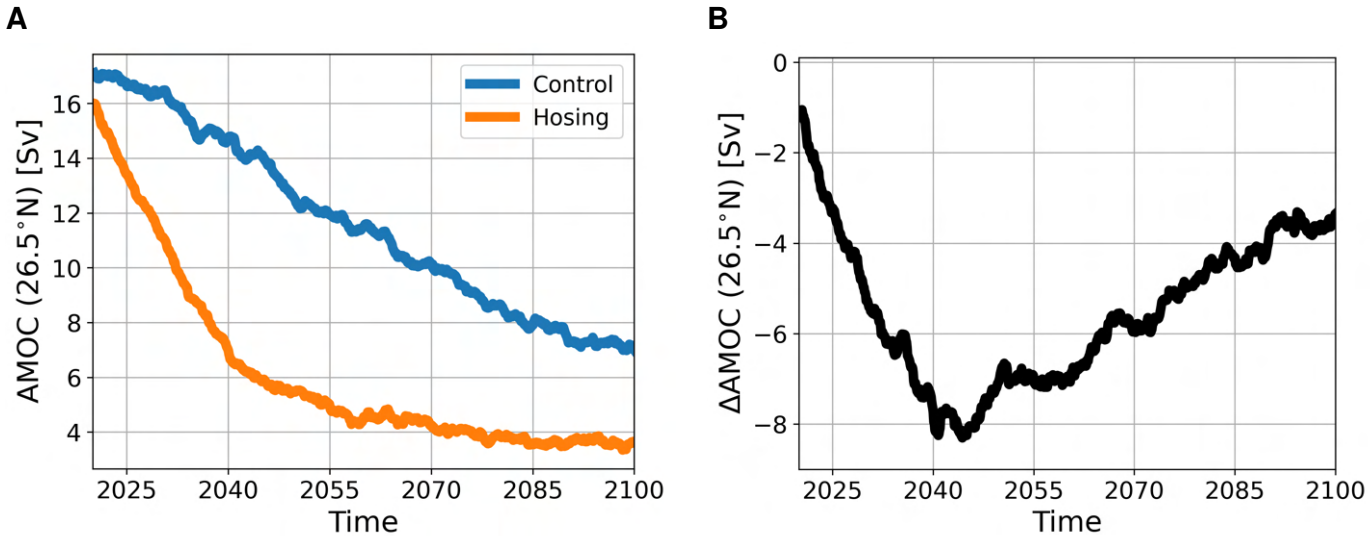

Figure 2. A. Atlantic Meridional Overturning Circulation strength at 26.5°N in Sverdrup (10^6 m^3 s^{-1}). Blue represents CTL-585 and orange HOS-585. B. The difference in AMOC strength between HOS-585 and CTL-585.

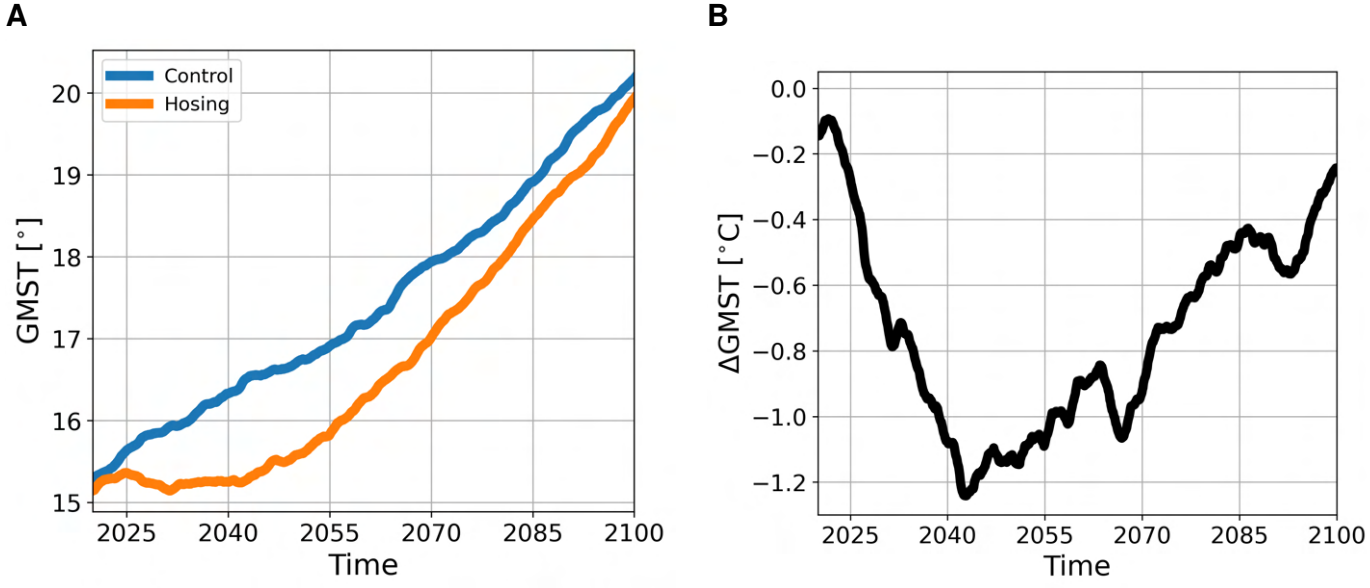

Figure 3. A. Global Mean Surface Temperature in °C for CTL-585 (blue) and HOS-585 (orange). B. The difference in GMST between HOS-585 and CTL-585.

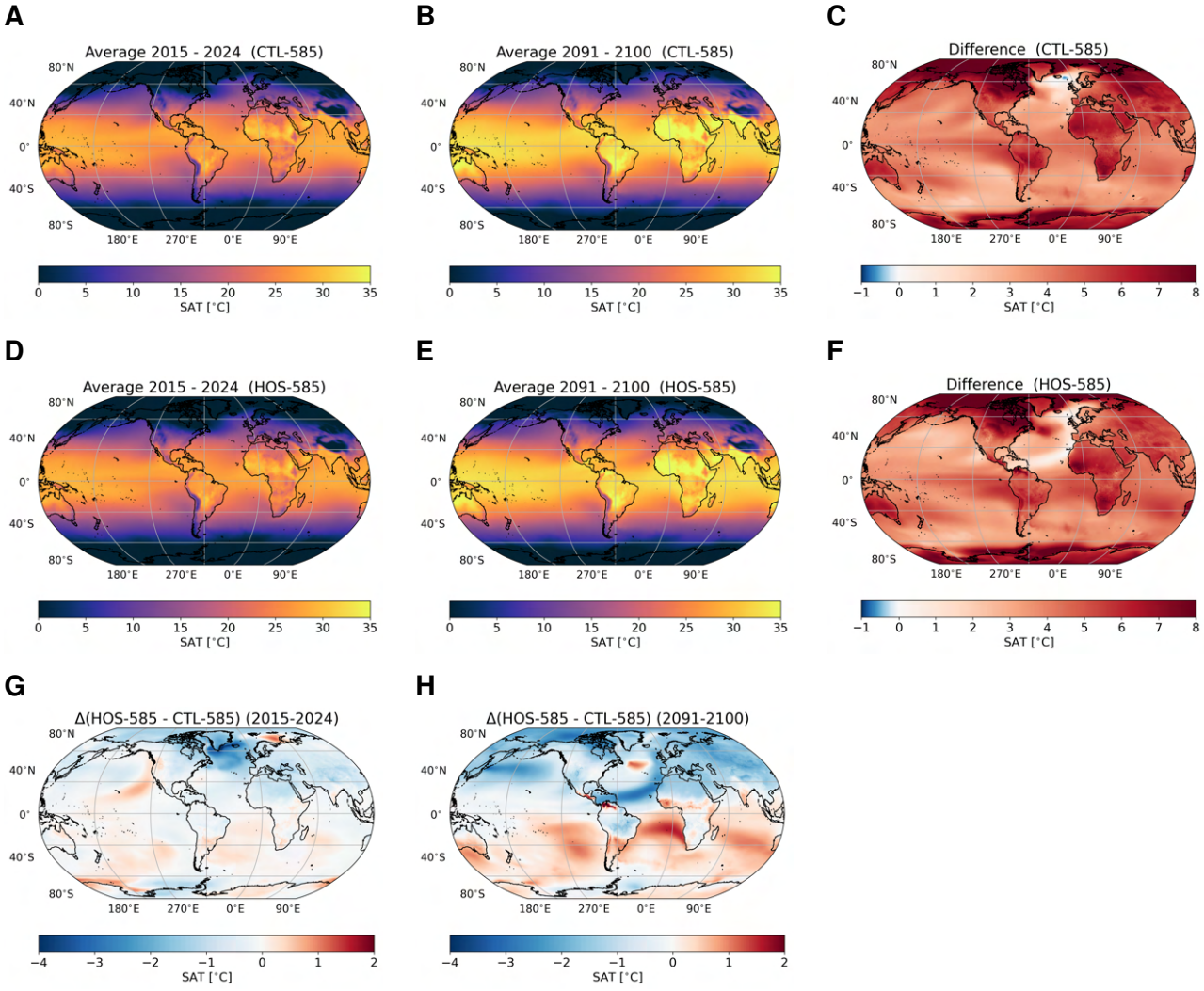

Figure 4. Surface Air Temperature (SAT) in °C for CTL-585 and HOS-585 and the difference between the two. The top row represents CTL-585 (A-C), the middle row HOS-585 (D-F), and the bottom row the difference (HOS-585 minus CTL-585; G, H). The left column represents the first decade (2015-2024; A, D, G), the middle column the last decade (2091-2100; B, E, H), and the right column the difference (last minus first; C, F).

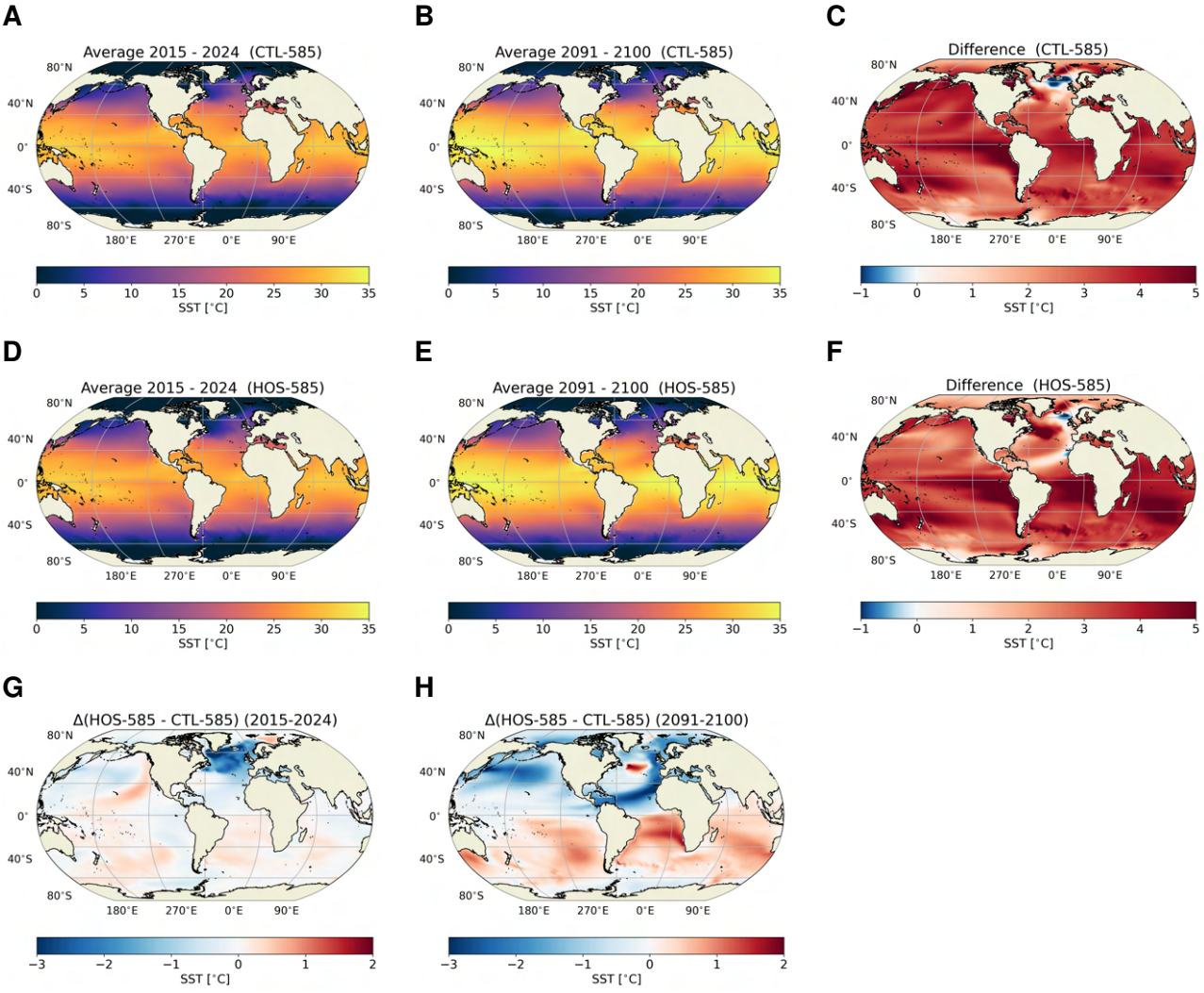

Figure 5. Sea Surface Temperature (SST) in °C for CTL-585 and HOS-585 and the difference between the two. The top row represents CTL-585 (A-C), the middle row HOS-585 (D-F), and the bottom row the difference (HOS-585 minus CTL-585; G, H). The left column represents the first decade (2015-2024; A, D, G), the middle column the last decade (2091-2100; B, E, H), and the right column the difference (last minus first; C, F).

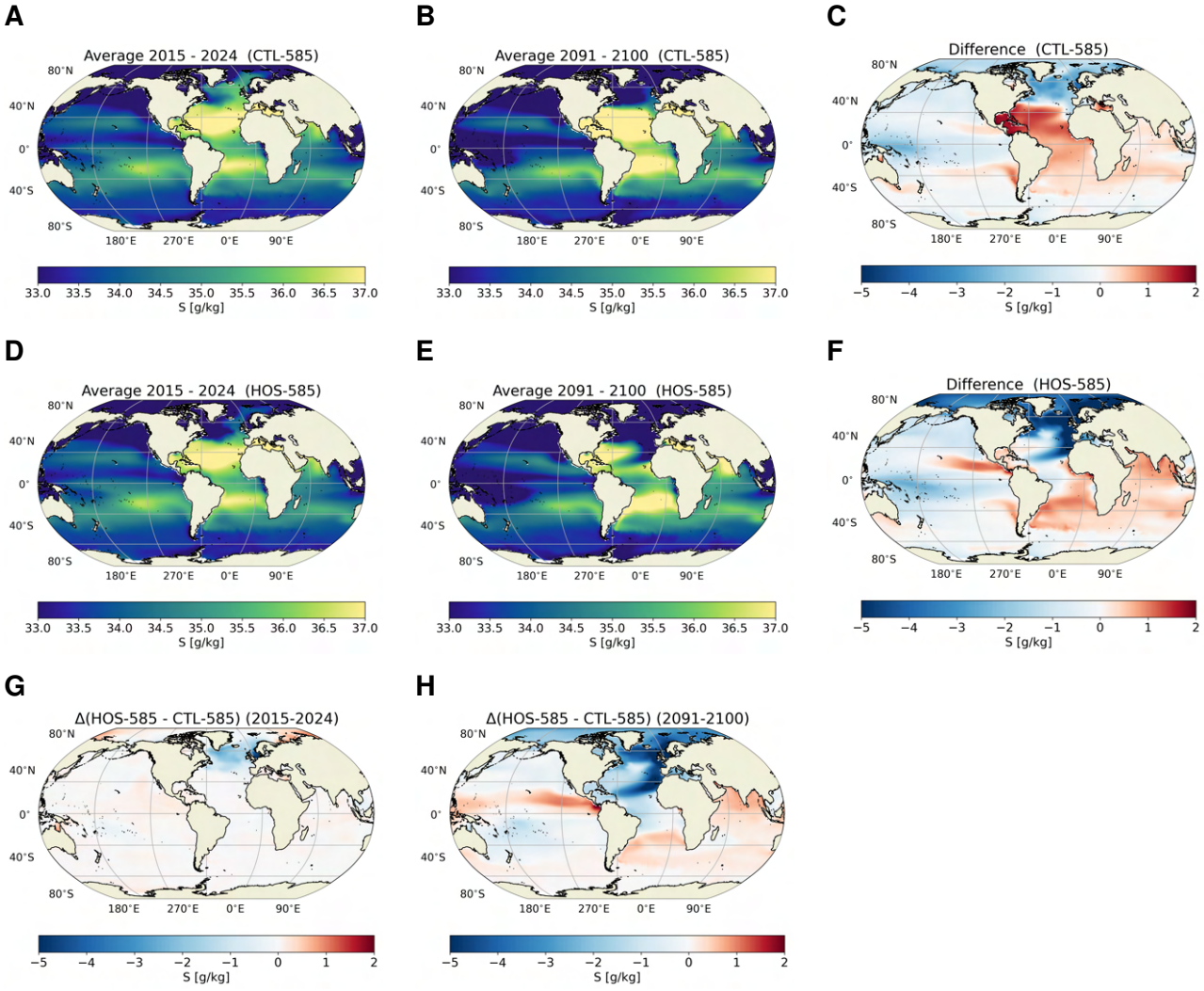

Figure 6. Sea Surface Salinity (S) in g kg^{-1} for CTL-585 and HOS-585 and the difference between the two. The top row represents CTL-585 (A-C), the middle row HOS-585 (D-F), and the bottom row the difference (HOS-585 minus CTL-585; G, H). The left column represents the first decade (2015-2024; A, D, G), the middle column the last decade (2091-2100; B, E, H), and the right column the difference (last minus first; C, F).

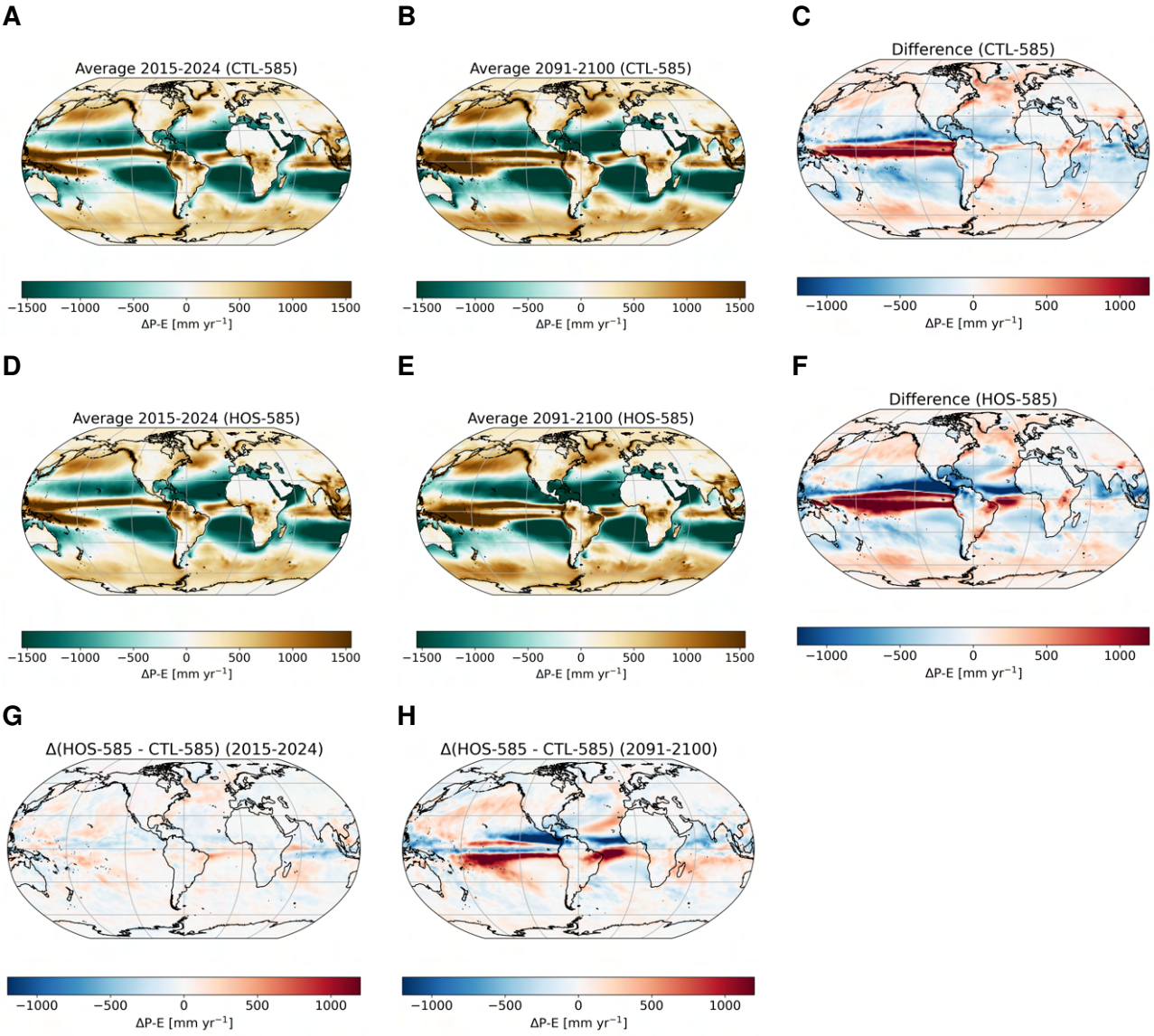

Figure 7. Net precipitation (precipitation minus evaporation; P-E) in mm year^{-1} for CTL-585 and HOS-585 and the difference between the two. The top row represents CTL-585 (A-C), the middle row HOS-585 (D-F), and the bottom row the difference (HOS-585 minus CTL-585; G, H). The left column represents the first decade (2015-2024; A, D, G), the middle column the last decade (2091-2100; B, E, H), and the right column the difference (last minus first; C, F).

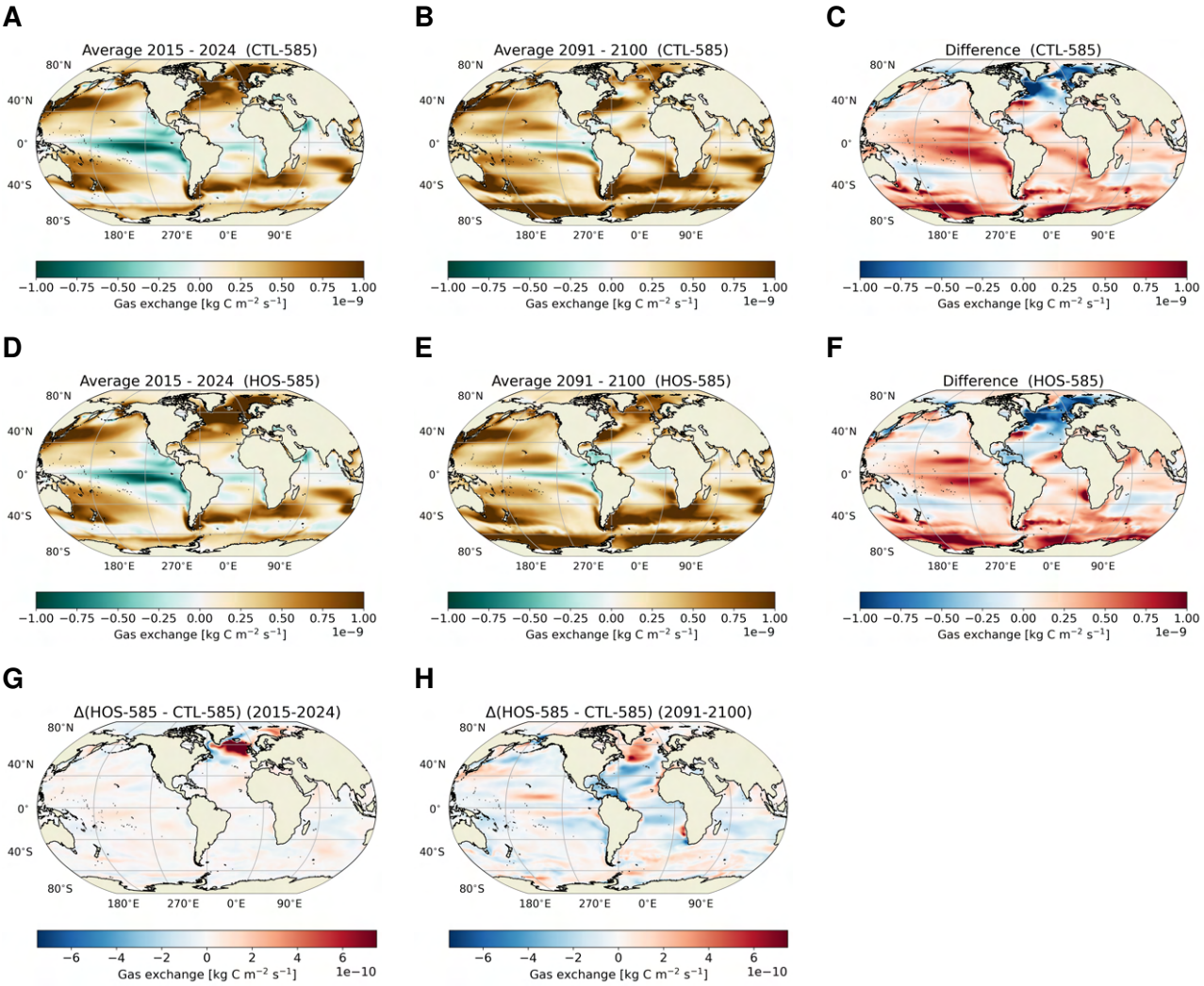

Figure 8. The air-sea gas exchange of CO_2 in kg C m^{-2} s^{-1} for CTL-585 and HOS-585 and the difference between the two. The top row represents CTL-585 (A-C), the middle row HOS-585 (D-F), and the bottom row the difference (HOS-585 minus CTL-585; G, H). The left column represents the first decade (2015-2024; A, D, G), the middle column the last decade (2091-2100; B, E, H), and the right column the difference (last minus first; C, F). Positive values in A, B, D and E represent fluxes going into the ocean.

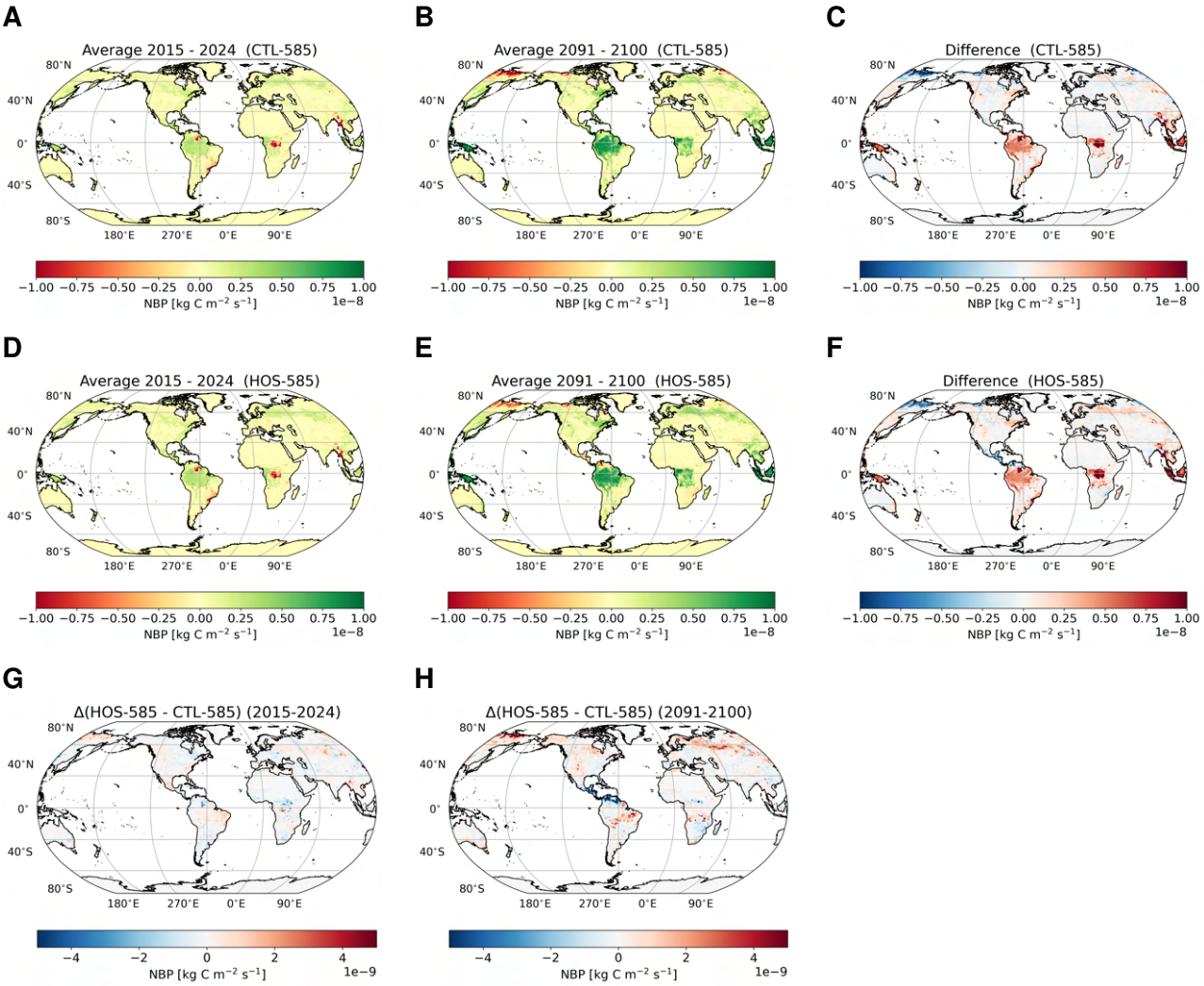

Figure 9. The air-land exchange of CO_2 in kg C m^{-2} s^{-1} for CTL-585 and HOS-585 and the difference between the two. The top row represents CTL-585 (A-C), the middle row HOS-585 (D-F), and the bottom row the difference (HOS-585 minus CTL-585; G, H). The left column represents the first decade (2015-2024; A, D, G), the middle column the last decade (2091-2100; B, E, H), and the right column the difference (last minus first; C, F). Positive values in A, B, D and E represent fluxes going into the ocean.

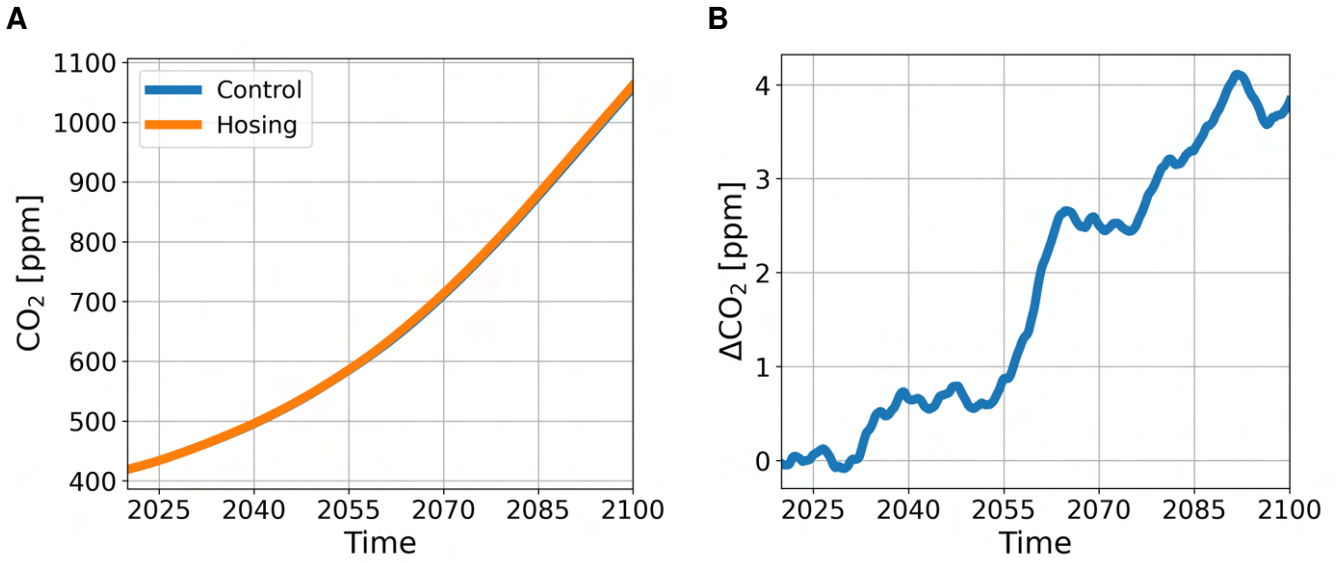

Figure 10. A. Atmospheric CO_2 concentration in ppm for CTL-585 (blue) and HOS-585 (orange). B. The difference in CO_2 concentration between HOS-585 and CTL-585.

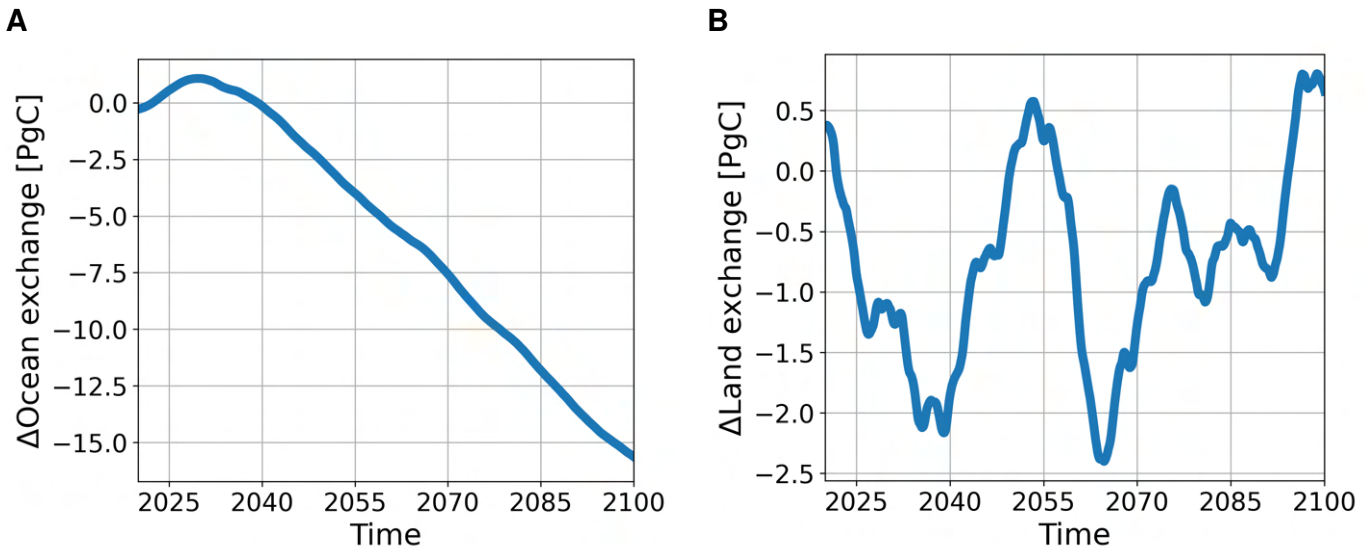

Figure 11. A. The difference in carbon exchange between the atmosphere and the ocean integrated globally and over time between HOS-585 and CTL-585. B. As in A but for the carbon exchange between the atmosphere and land.

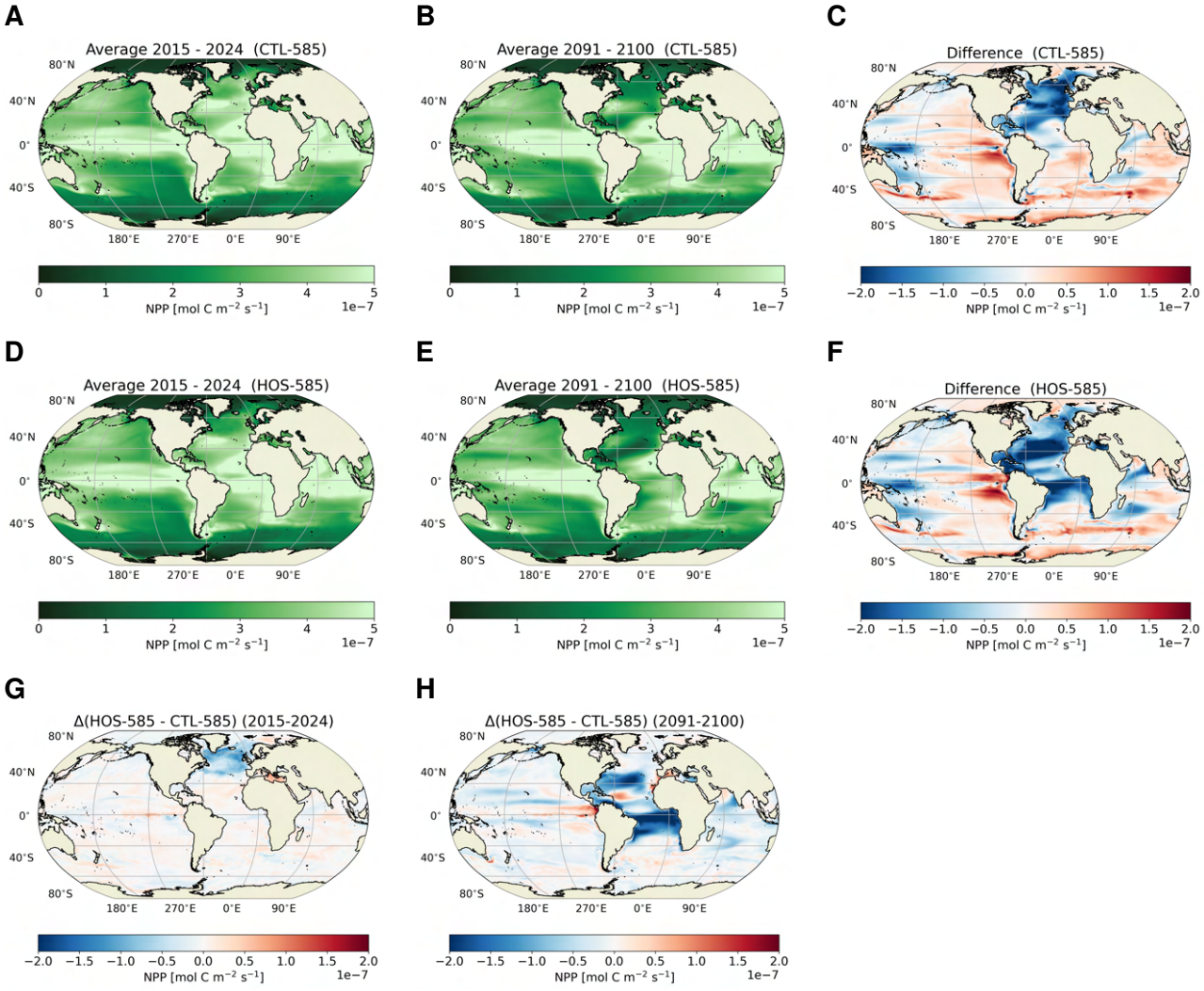

Figure 12. The Net Primary Production (NPP) integrated over the top 150 m of the ocean in mol C m^{-2} s^{-1} for CTL-585 and HOS-585 and the difference between the two. The top row represents CTL-585 (A-C), the middle row HOS-585 (D-F), and the bottom row the difference (HOS-585 minus CTL-585; G, H). The left column represents the first decade (2015-2024; A, D, G), the middle column the last decade (2091-2100; B, E, H), and the right column the difference (last minus first; C, F).

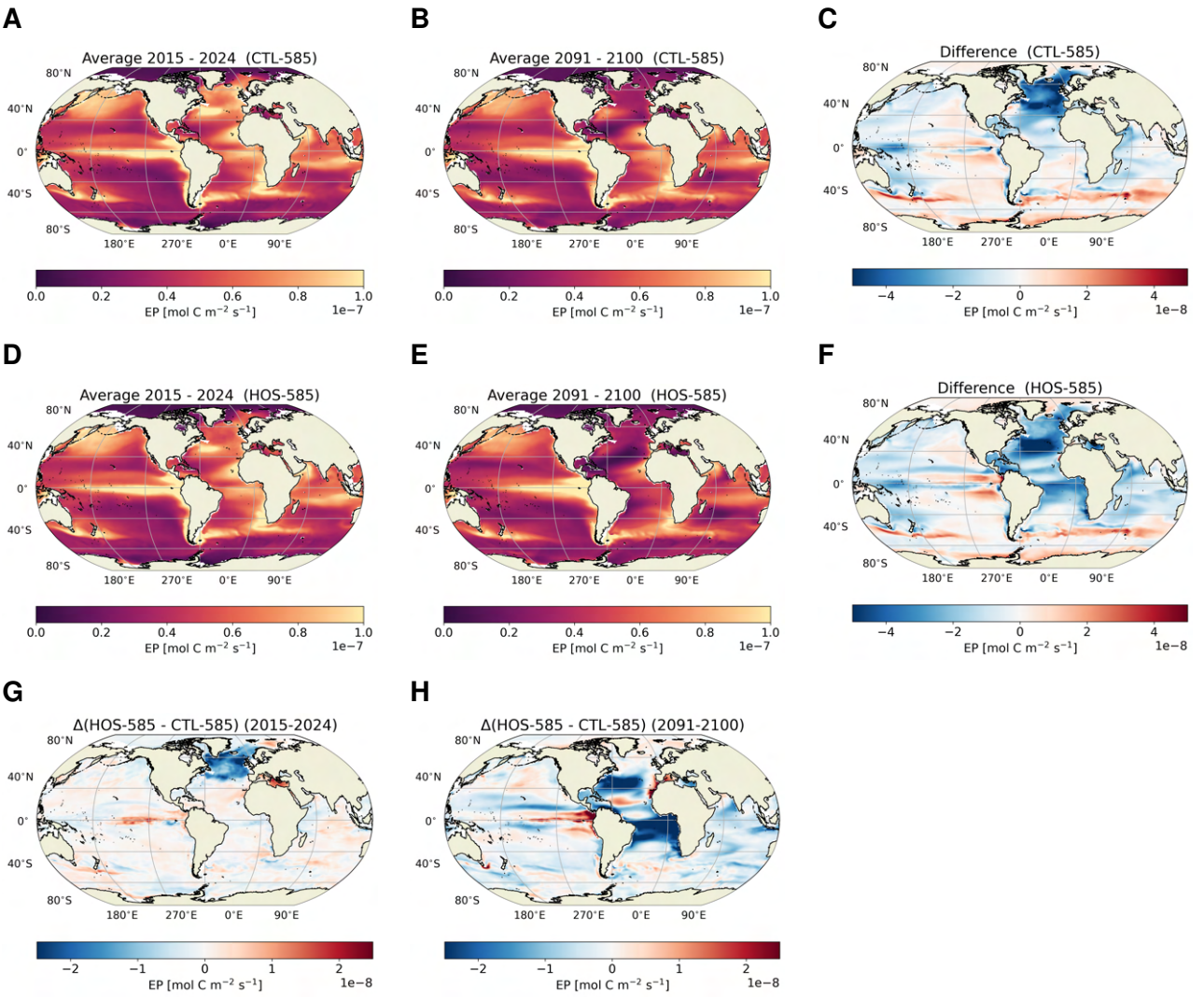

Figure 13. The Export Production (POC flux; EP) at 100 m depth in mol C m^{-2} s^{-1} for CTL-585 and HOS-585 and the difference between the two. The top row represents CTL-585 (A-C), the middle row HOS-585 (D-F), and the bottom row the difference (HOS-585 minus CTL-585; G, H). The left column represents the first decade (2015-2024; A, D, G), the middle column the last decade (2091-2100; B, E, H), and the right column the difference (last minus first; C, F).

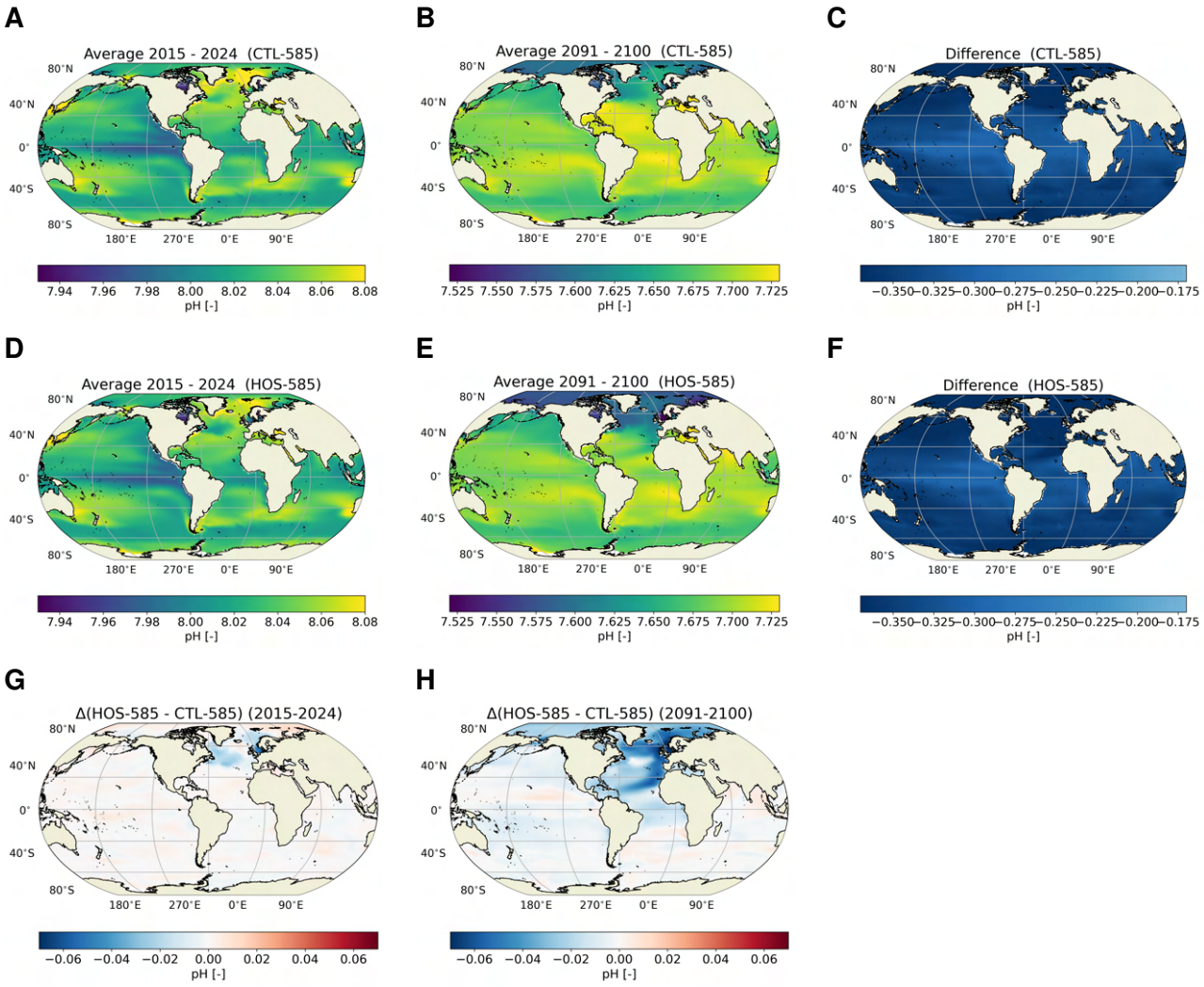

Figure 14. The pH of the surface ocean (unitless) for CTL-585 and HOS-585 and the difference between the two. The top row represents CTL-585 (A-C), the middle row HOS-585 (D-F), and the bottom row the difference (HOS-585 minus CTL-585; G, H). The left column represents the first decade (2015-2024; A, D, G), the middle column the last decade (2091-2100; B, E, H), and the right column the difference (last minus first; C, F).

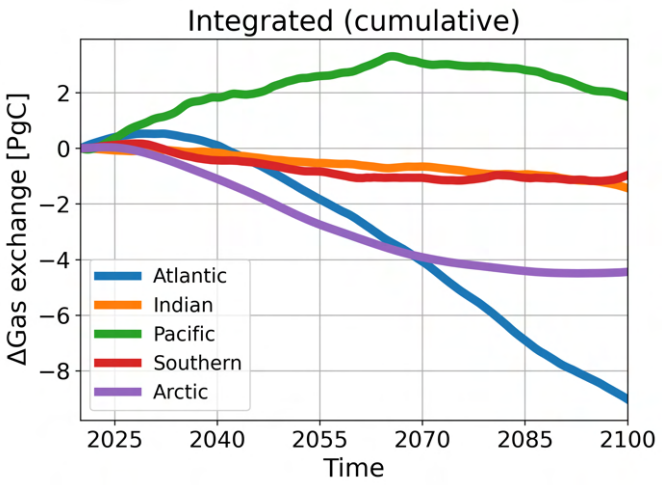

Figure 15. The difference between HOS-585 and CTL-585 for the exchange of CO_2 between the atmosphere and the ocean integrated over time and five different ocean basins in PgC: Atlantic Ocean (blue), Indian Ocean (orange), Pacific Ocean (green), Southern Ocean (red) and the Arctic Ocean (purple). The Southern Ocean is defined as the ocean south of 35°S, and the Arctic Ocean as the ocean north of 66°N.

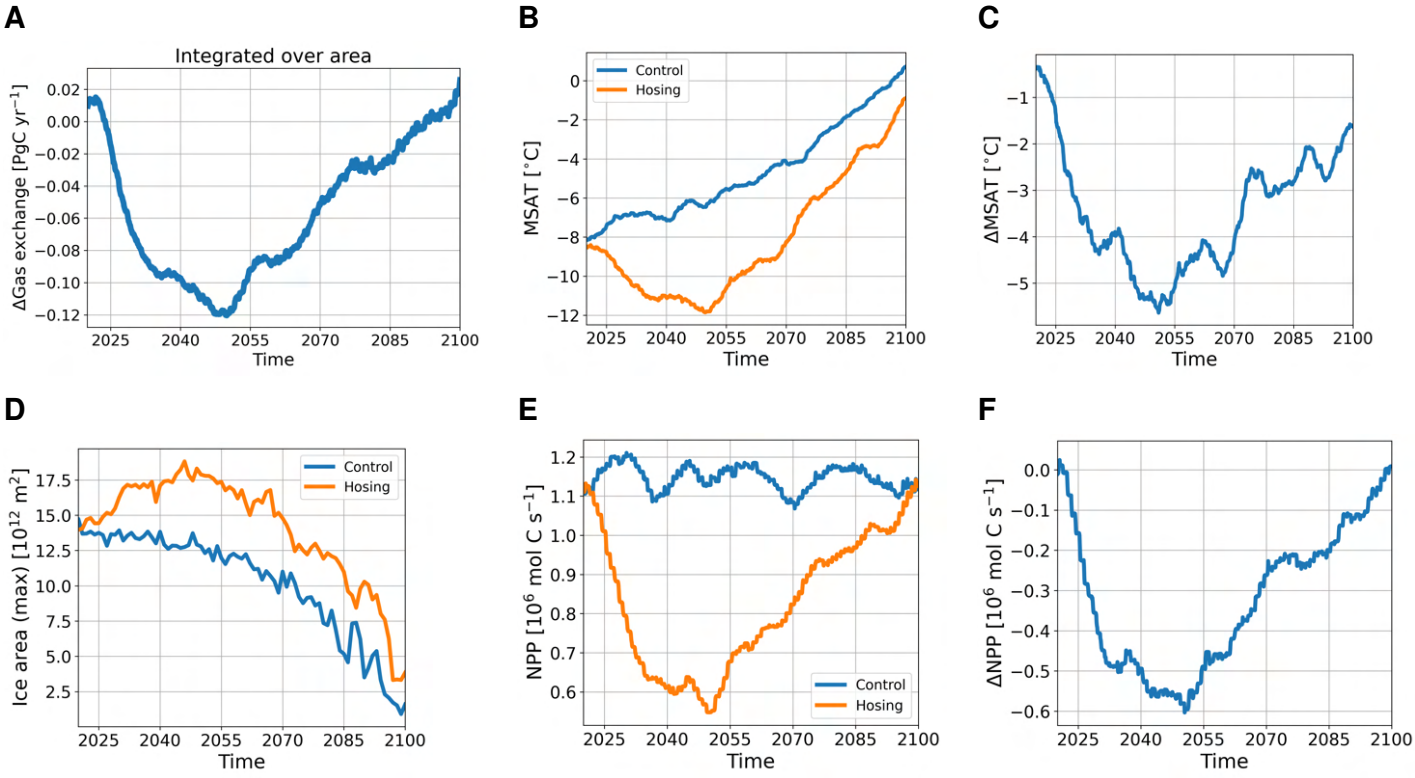

Figure 16. Several variables for the Arctic Ocean. A. The difference between HOS-585 and CTL-585 for the exchange of CO_2 between the atmosphere and the Arctic Ocean in PgC yr^{-1}. B. Mean Surface Air Temperature (MSAT) in °C above the Arctic Ocean for CTL-585 (blue) and HOS-585 (orange). C. The difference in MSAT between HOS-585 and CTL-585 shown in B. D. The yearly maximum areal sea ice extent in 10^{12} m^2 for CTL-585 (blue) and HOS-585 (orange). E. Net Primary Production integrated over the top 150 m of the ocean in 10^6 mol C m^{-2} s^{-1} for CTL-585 (blue) and HOS-585 (orange). F. The difference in NPP between HOS-585 and CTL-585 as shown in E.

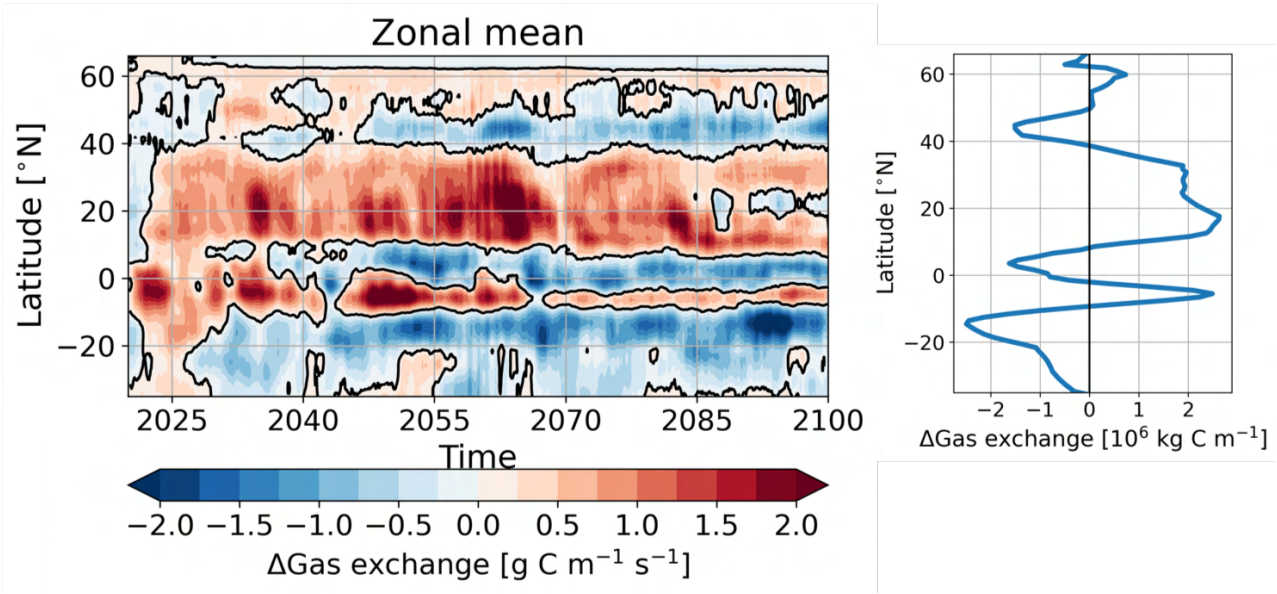

Figure 17. A. Hovmoller diagram of the difference between HOS-585 and CTL-585 for the air-sea gas exchange of CO_2 for the Pacific basin presented as zonal means in kg C m^{-1} s^{-1}. B. As in A but also integrated over time in 10^6 kg C m^{-1}.

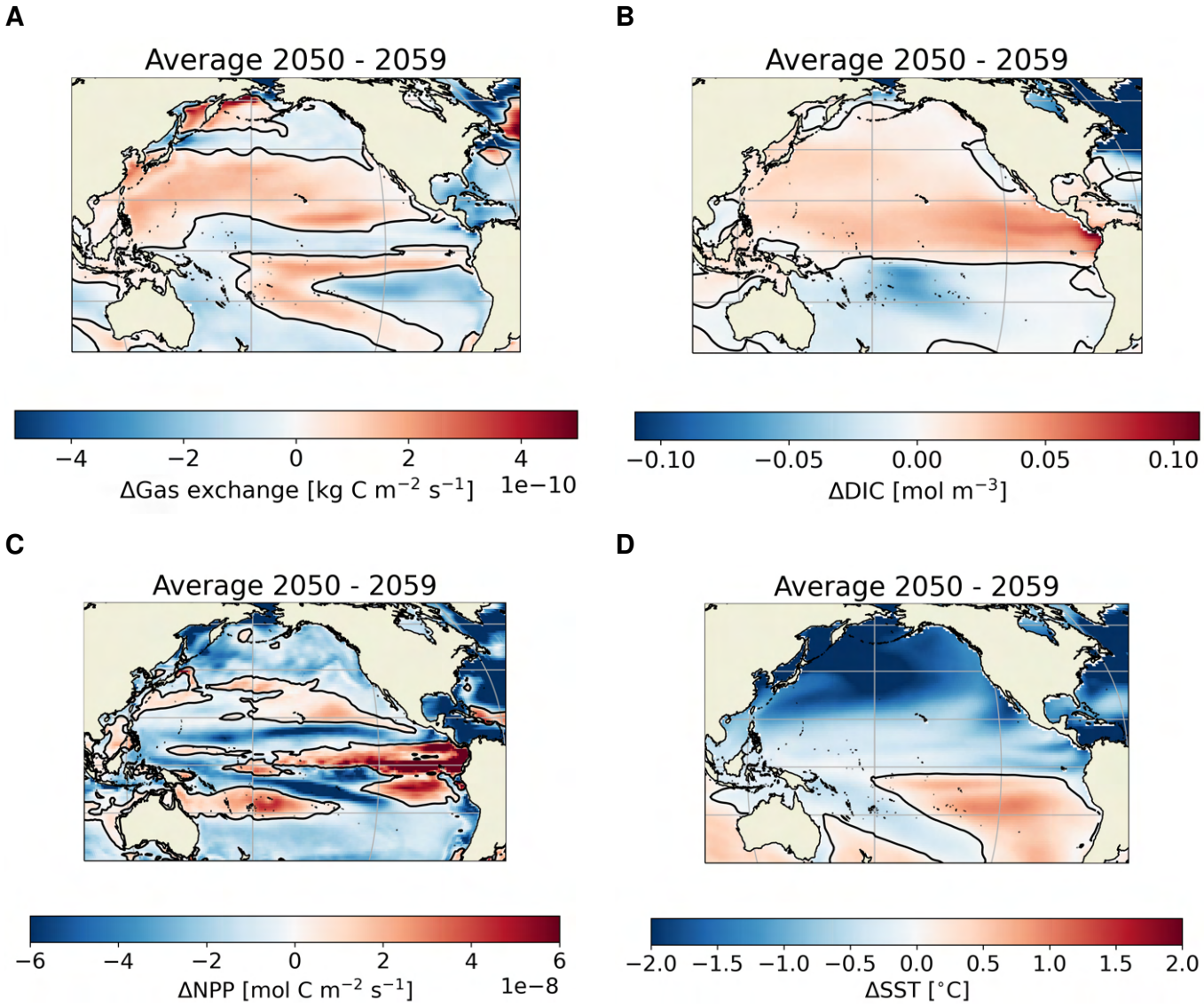

Figure 18. Several variables for the Pacific Ocean averaged over the period 2050-2059 (mid-simulation). All figures display the difference between HOS-585 and CTL-585. A. The air-sea gas exchange of CO_2 in kg C m^{-2} s^{-1}. B. Surface Dissolved Inorganic Carbon (DIC) concentration in mol m^{-3}. C. Net Primary Production (NPP) integrated over the top 150 m in mol C m^{-2} s^{-1}. D. Sea surface temperature (SST) in °C.

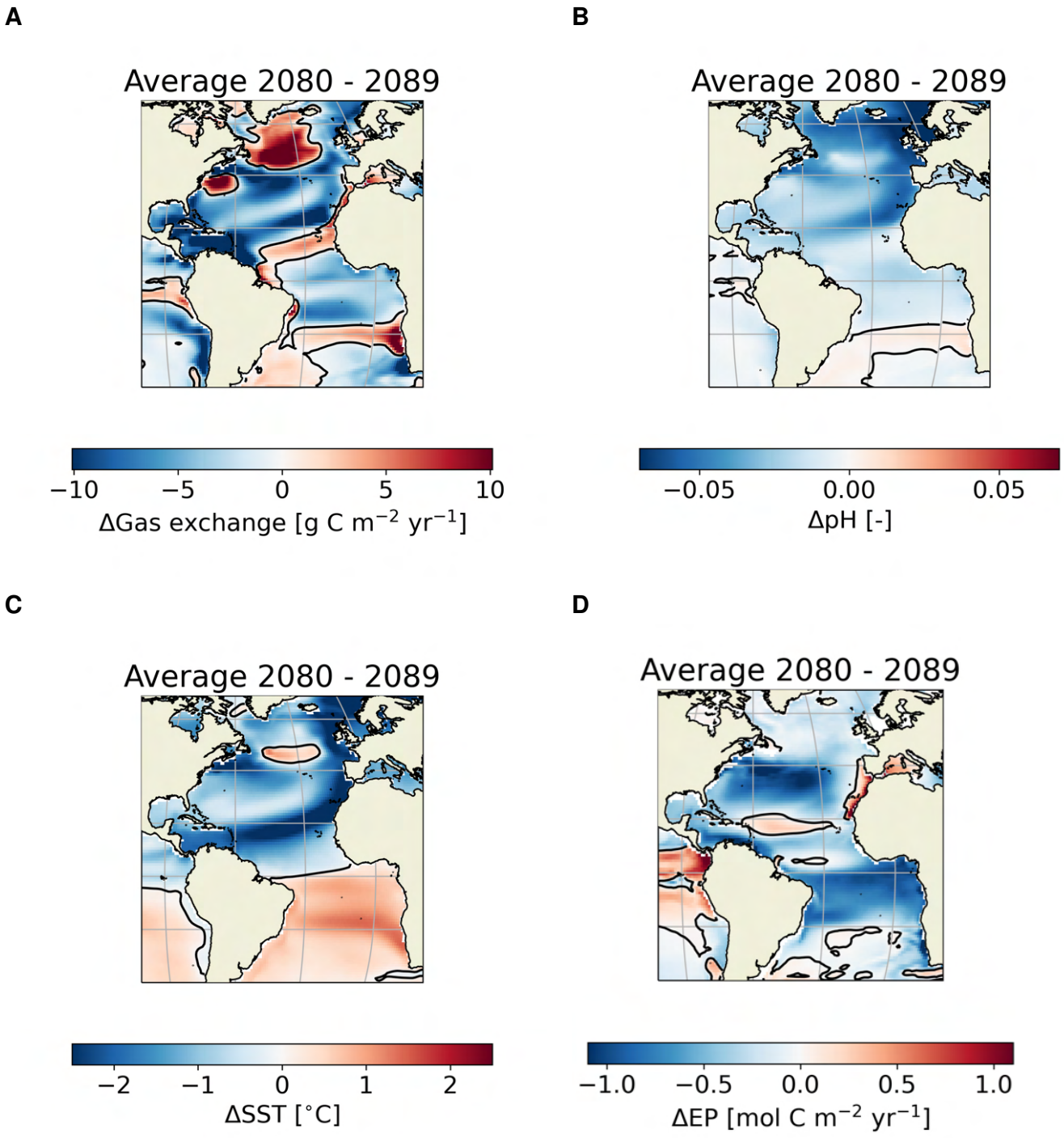

Figure 19. Several variables for the Atlantic Ocean averaged over the period 2080-2089 (mid-simulation). All figures display the difference between HOS-585 and CTL-585. A. The air-sea gas exchange of CO_2 in kg C m^{-2} s^{-1}. B. Surface pH (unitless). C. Sea surface temperature (SST) in °C. D. Export Production (POC flux; EP) at 100 m depth in mol C m^{-2} s^{-1}.

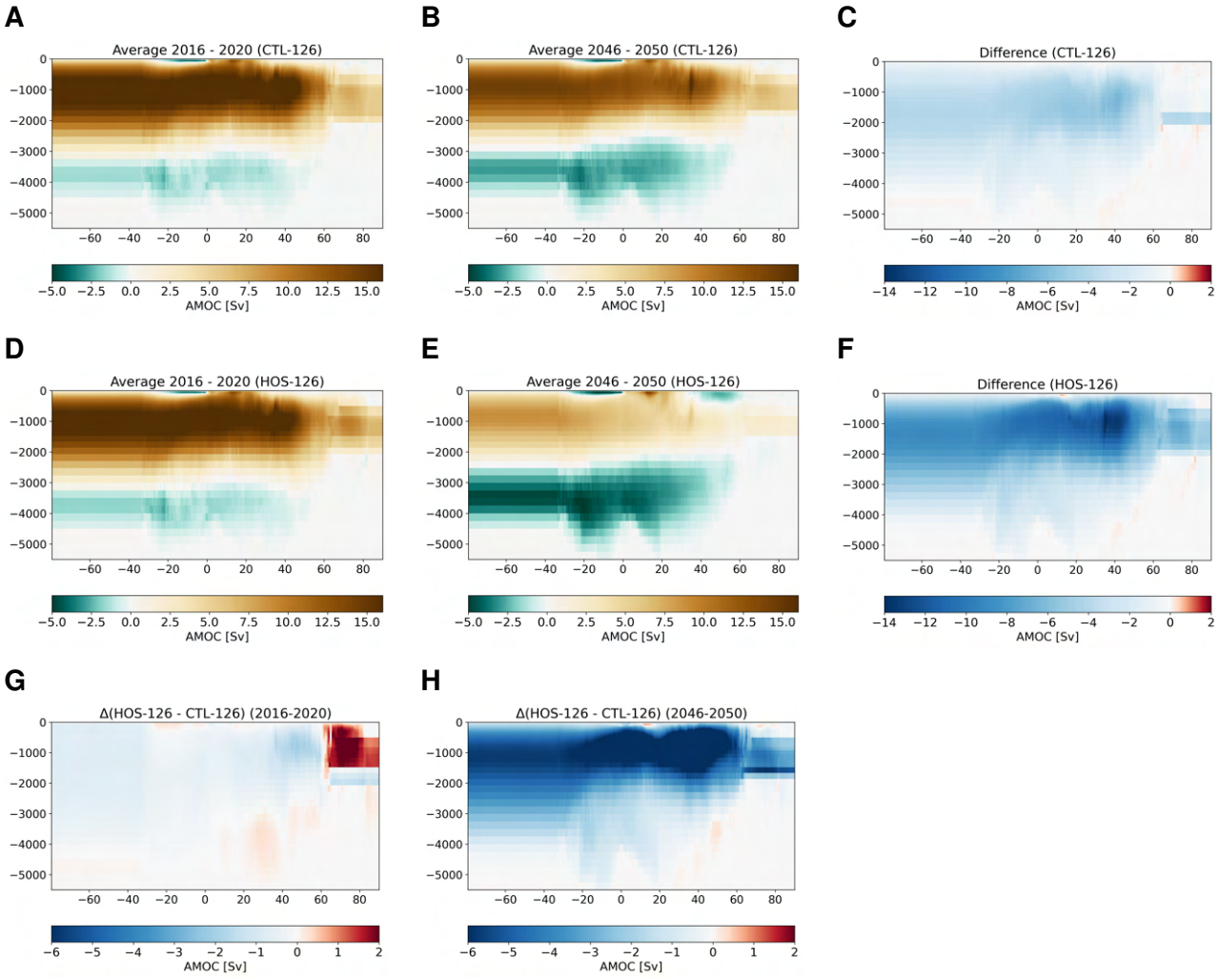

Figure 20. Atlantic Meridional Overturning Circulation streamfunction in Sverdrup (10^6 m^3 s^{-1}) for CTL-126 and HOS-126 and the difference between the two. The top row represents CTL-126 (A-C), the middle row HOS-126 (D-F), and the bottom row the difference (HOS-126 minus CTL-126; G, H). The left column represents the first decade (2015-2024; A, D, G), the middle column the last decade (2091-2100; B, E, H), and the right column the difference (last minus first; C, F).

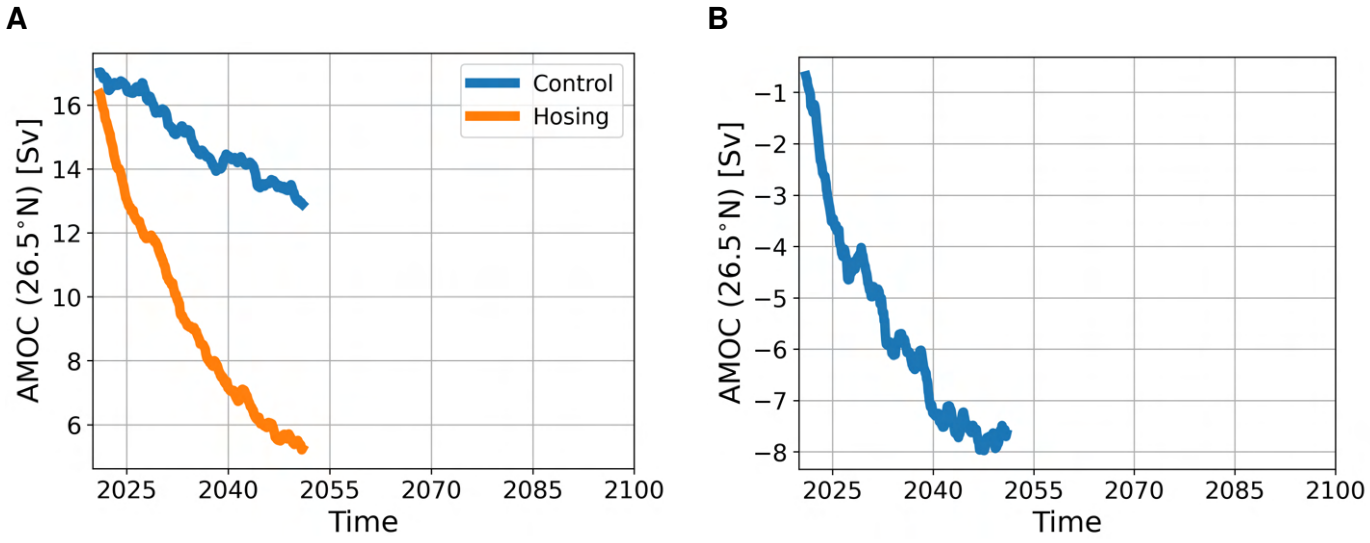

Figure 21. A. Atlantic Meridional Overturning Circulation strength at 26.5°N in Sverdrup (10^6 m^3 s^{-1}). Blue represents CTL-126 and orange HOS-126. B. The difference in AMOC strength between HOS-126 and CTL-126.

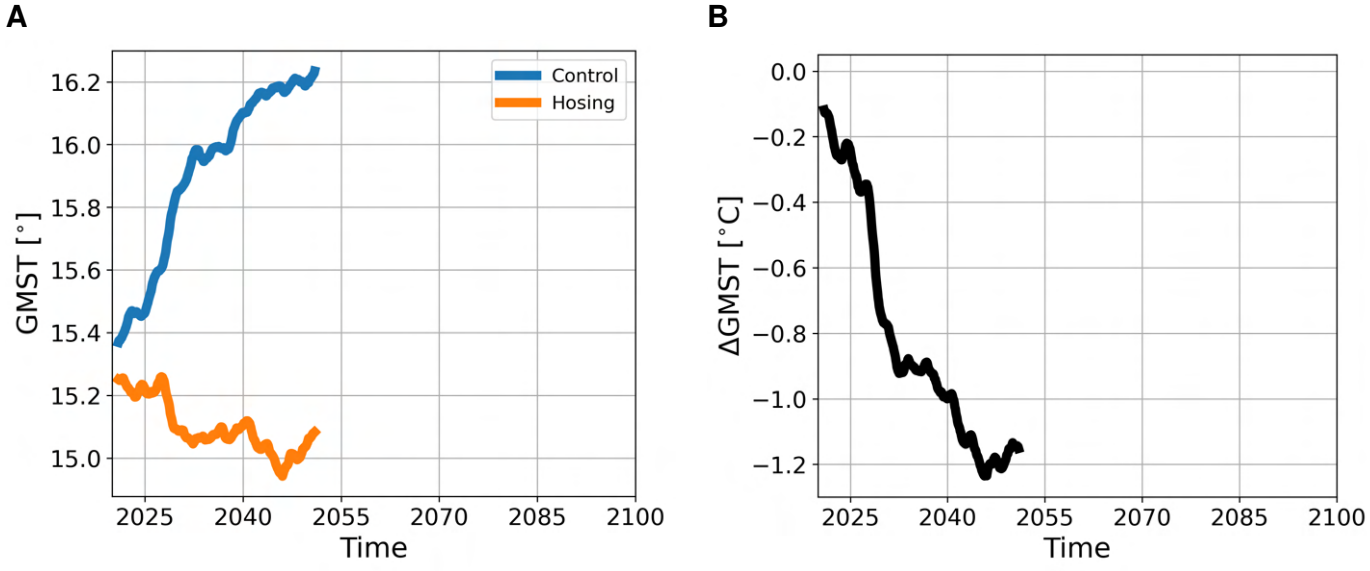

Figure 22. A. Global Mean Surface Temperature in °C for CTL-126 (blue) and HOS-126 (orange). B. The difference in GMST between HOS-126 and CTL-126.

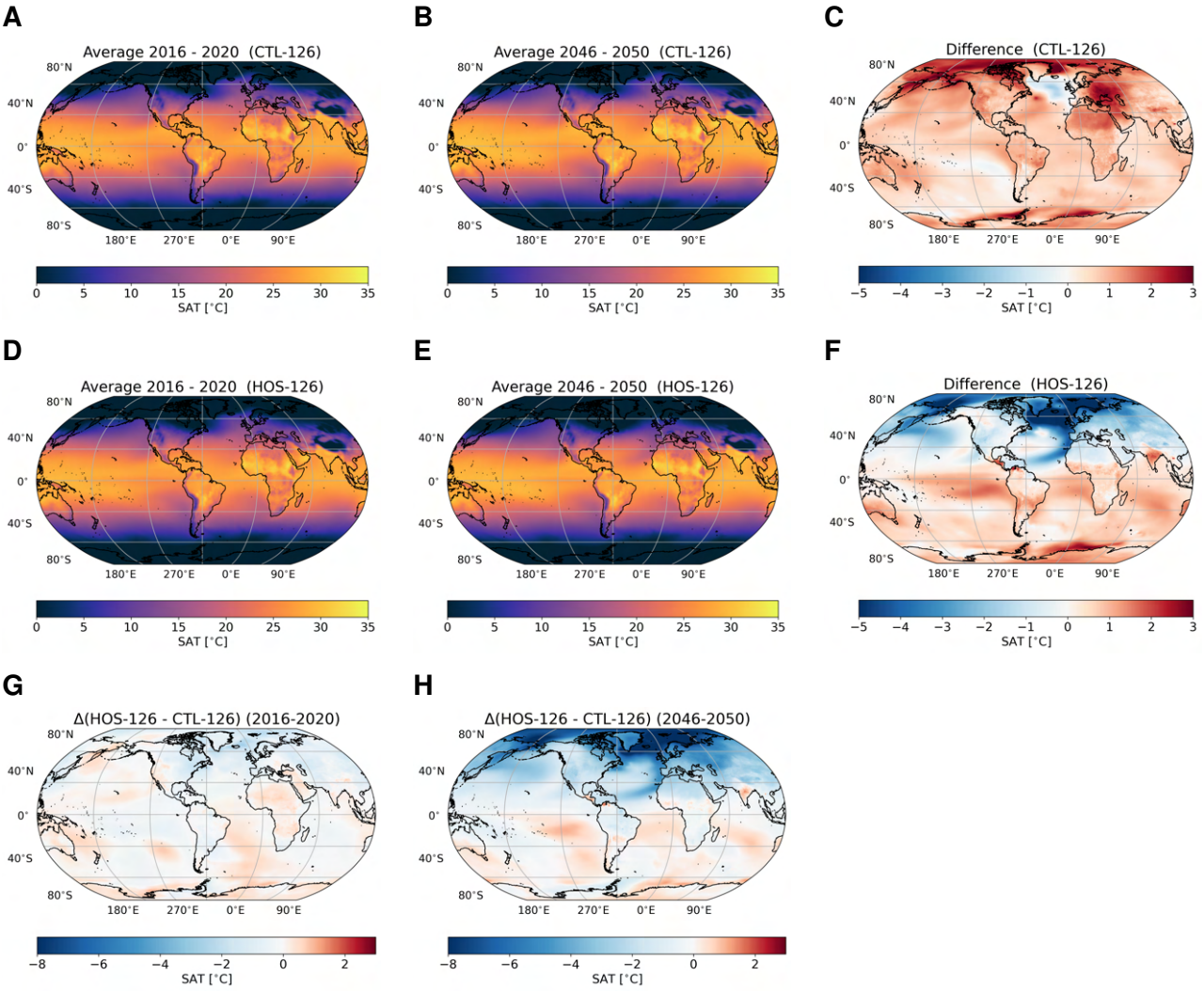

Figure 23. Surface Air Temperature (SAT) in °C for CTL-126 and HOS-126 and the difference between the two. The top row represents CTL-126 (A-C), the middle row HOS-126 (D-F), and the bottom row the difference (HOS-126 minus CTL-126; G, H). The left column represents the first decade (2015-2024; A, D, G), the middle column the last decade (2091-2100; B, E, H), and the right column the difference (last minus first; C, F).

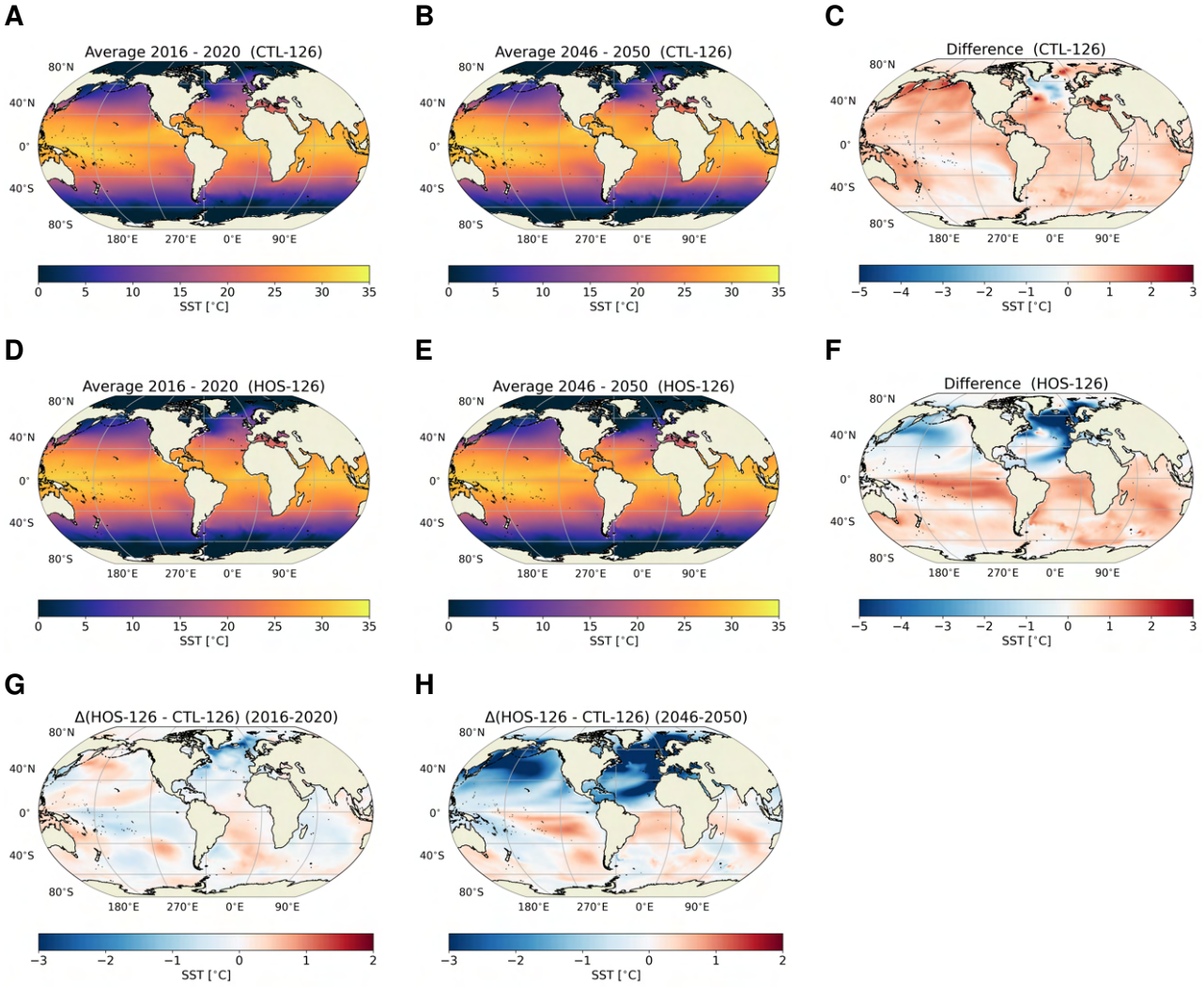

Figure 24. Sea Surface Temperature (SST) in °C for CTL-126 and HOS-126 and the difference between the two. The top row represents CTL-126 (A-C), the middle row HOS-126 (D-F), and the bottom row the difference (HOS-126 minus CTL-126; G, H). The left column represents the first decade (2015-2024; A, D, G), the middle column the last decade (2091-2100; B, E, H), and the right column the difference (last minus first; C, F).

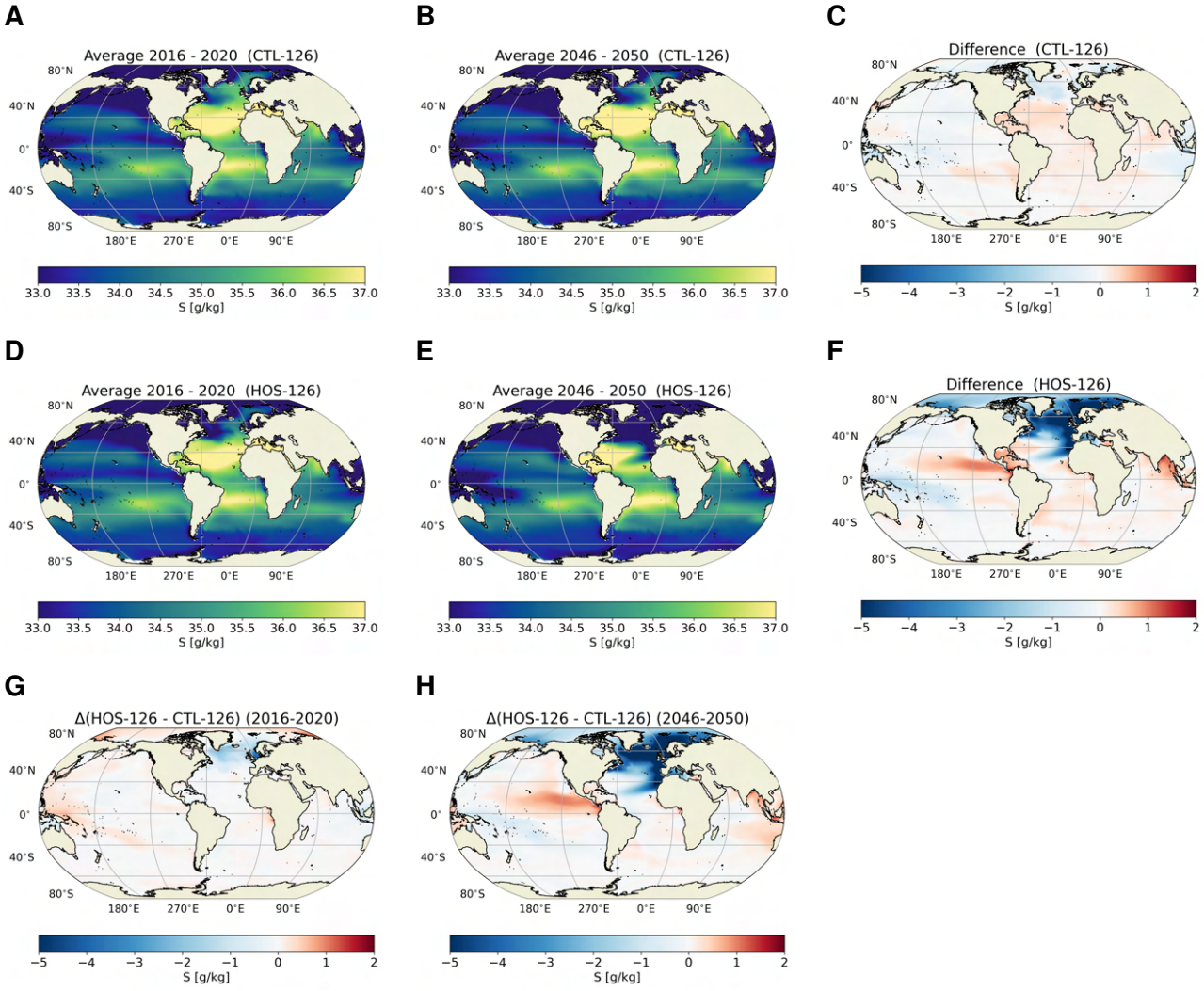

Figure 25. Sea Surface Salinity (S) in g kg^{-1} for CTL-126 and HOS-126 and the difference between the two. The top row represents CTL-126 (A-C), the middle row HOS-126 (D-F), and the bottom row the difference (HOS-126 minus CTL-126; G, H). The left column represents the first decade (2015-2024; A, D, G), the middle column the last decade (2091-2100; B, E, H), and the right column the difference (last minus first; C, F).

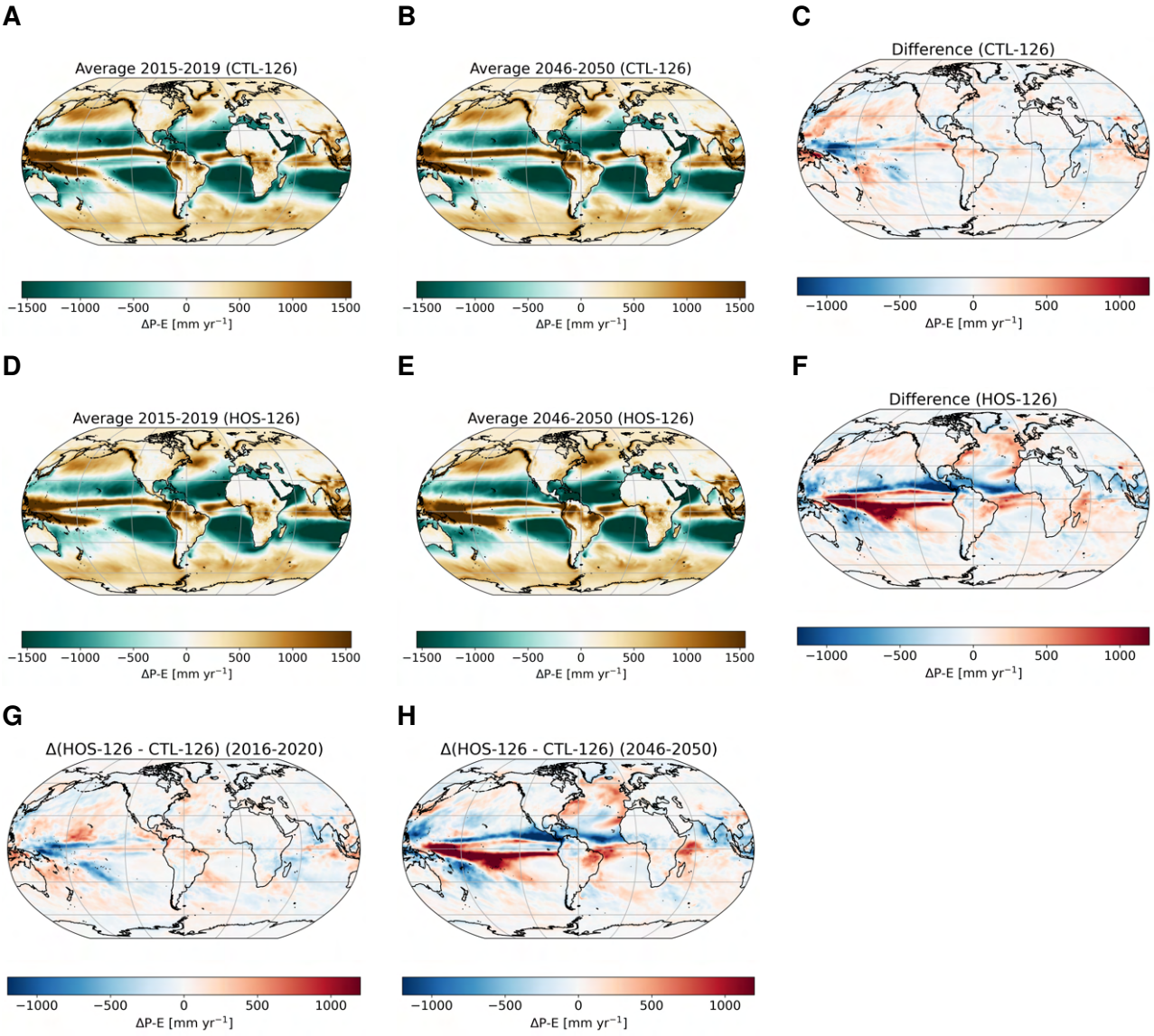

Figure 26. Net precipitation (precipitation minus evaporation; P-E) in mm year^{-1} for CTL-126 and HOS-126 and the difference between the two. The top row represents CTL-126 (A-C), the middle row HOS-126 (D-F), and the bottom row the difference (HOS-126 minus CTL-126; G, H). The left column represents the first decade (2015-2024; A, D, G), the middle column the last decade (2091-2100; B, E, H), and the right column the difference (last minus first; C, F).

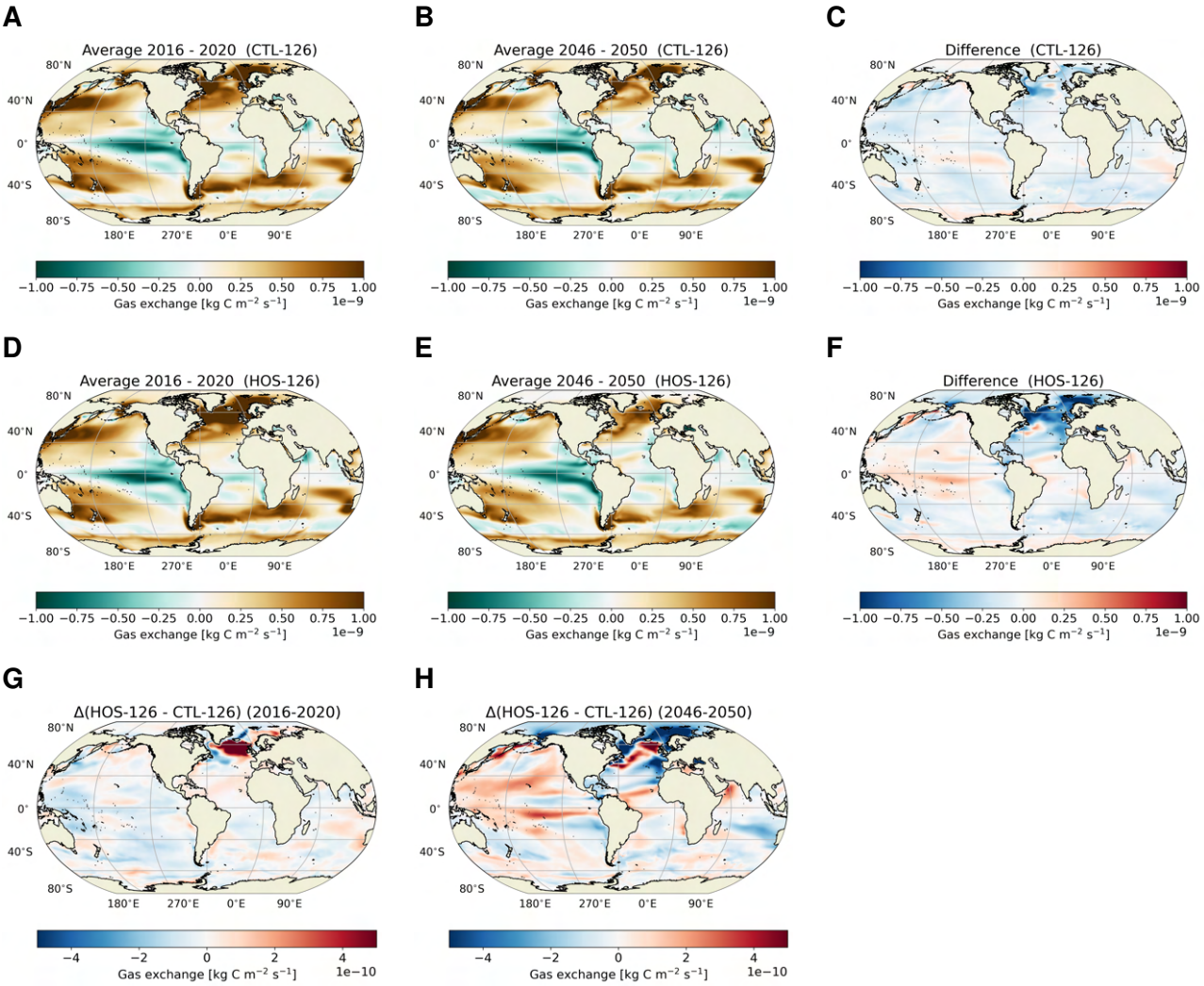

Figure 27. The air-sea gas exchange of CO_2 in kg C m^{-2} s^{-1} for CTL-126 and HOS-126 and the difference between the two. The top row represents CTL-126 (A-C), the middle row HOS-126 (D-F), and the bottom row the difference (HOS-126 minus CTL-126; G, H). The left column represents the first decade (2015-2024; A, D, G), the middle column the last decade (2091-2100; B, E, H), and the right column the difference (last minus first; C, F). Positive values in A, B, D and E represent fluxes going into the ocean.

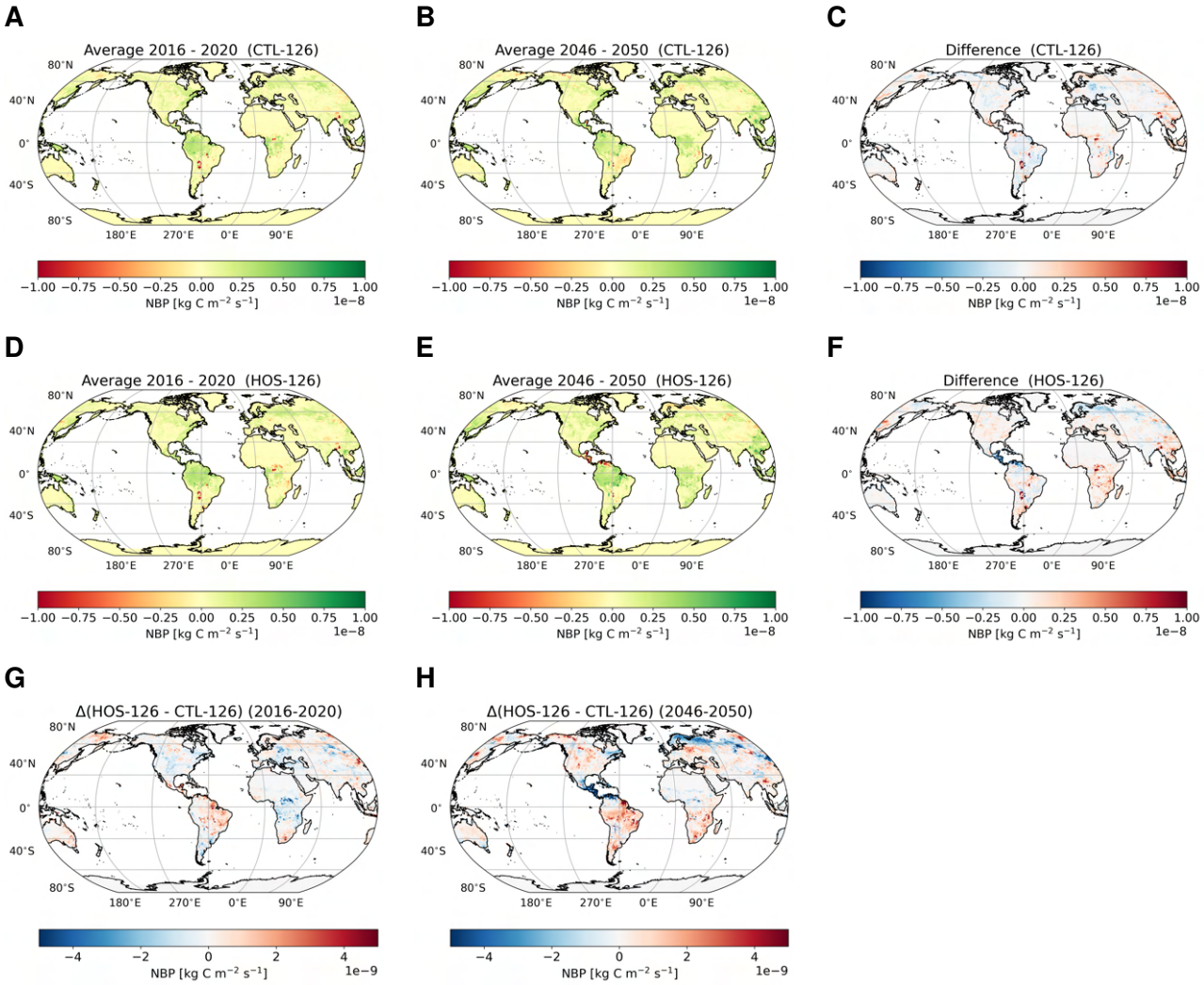

Figure 28. The air-land exchange of CO_2 in kg C m^{-2} s^{-1} for CTL-126 and HOS-126 and the difference between the two. The top row represents CTL-126 (A-C), the middle row HOS-126 (D-F), and the bottom row the difference (HOS-126 minus CTL-126; G, H). The left column represents the first decade (2015-2024; A, D, G), the middle column the last decade (2091-2100; B, E, H), and the right column the difference (last minus first; C, F). Positive values in A, B, D and E represent fluxes going into the ocean.

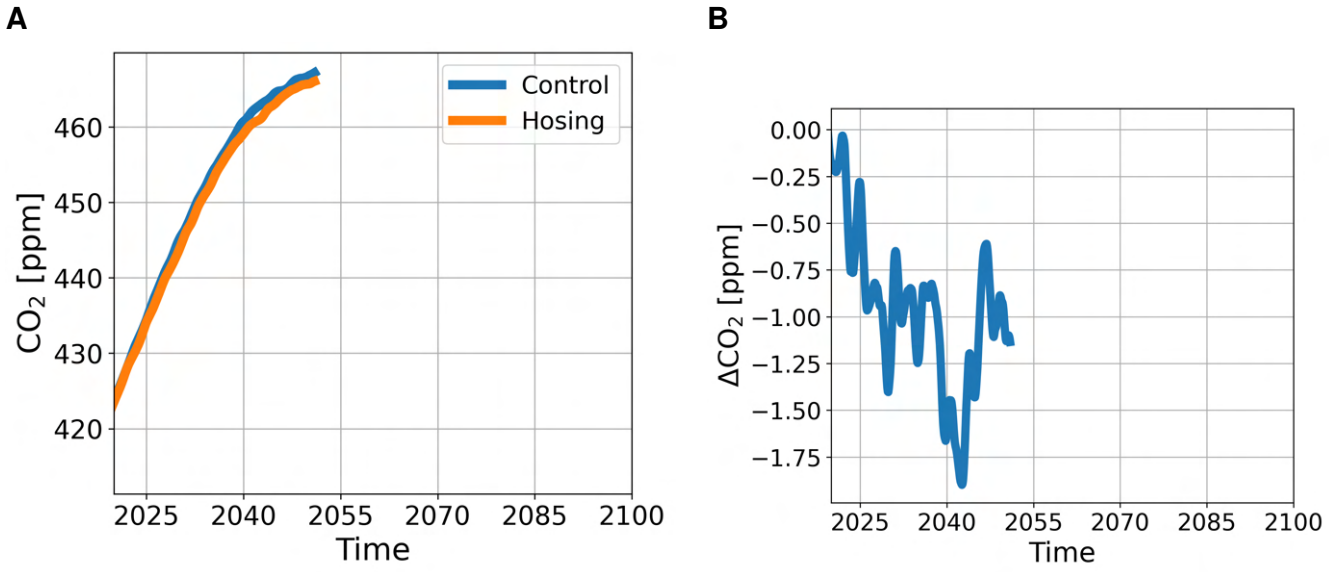

Figure 29. A. Atmospheric CO_2 concentration in ppm for CTL-126 (blue) and HOS-126 (orange). B. The difference in CO_2 concentration between HOS-126 and CTL-126.

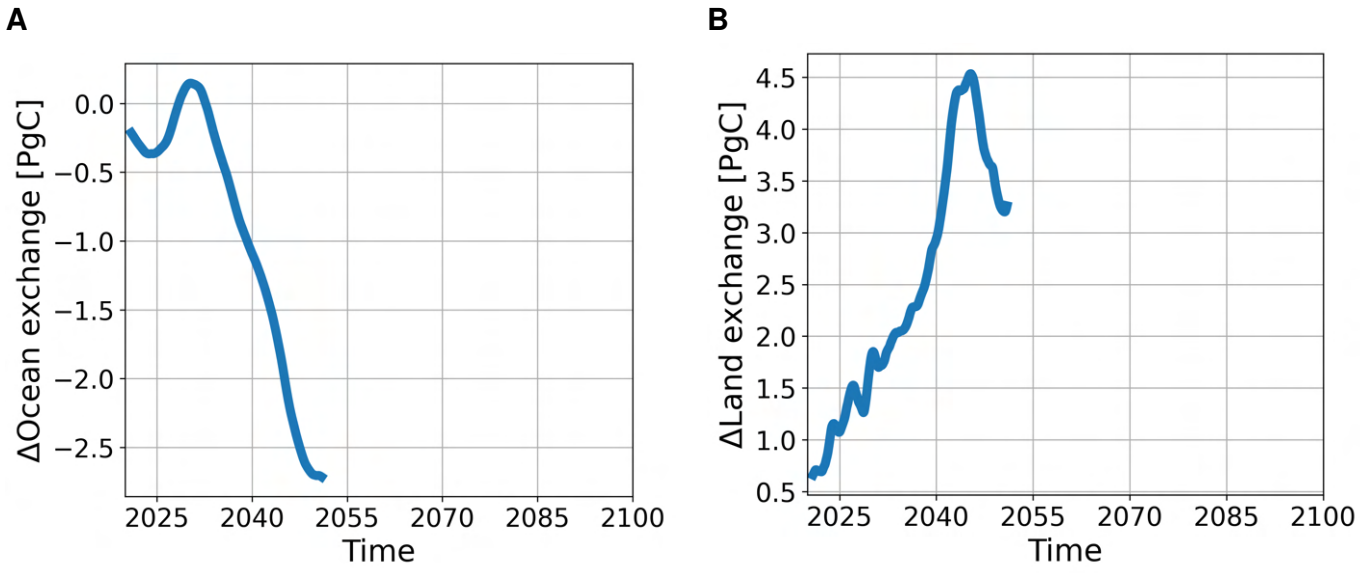

Figure 30. A. The difference in carbon exchange between the atmosphere and the ocean integrated globally and over time between HOS-126 and CTL-126. B. As in A but for the carbon exchange between the atmosphere and land.

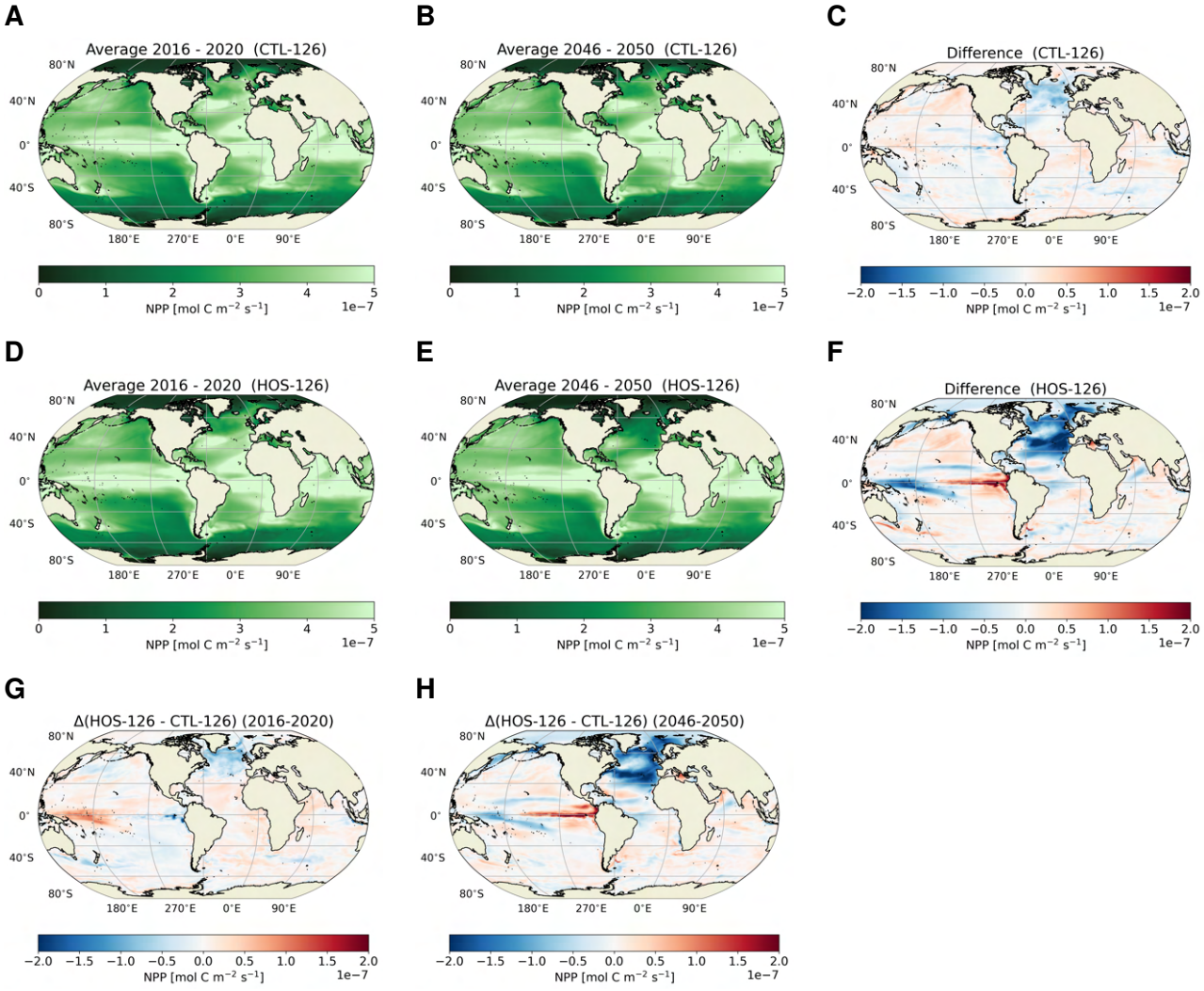

Figure 31. The Net Primary Production (NPP) integrated over the top 150 m of the ocean in mol C m^{-2} s^{-1} for CTL-126 and HOS-126 and the difference between the two. The top row represents CTL-126 (A-C), the middle row HOS-126 (D-F), and the bottom row the difference (HOS-126 minus CTL-126; G, H). The left column represents the first decade (2015-2024; A, D, G), the middle column the last decade (2091-2100; B, E, H), and the right column the difference (last minus first; C, F).

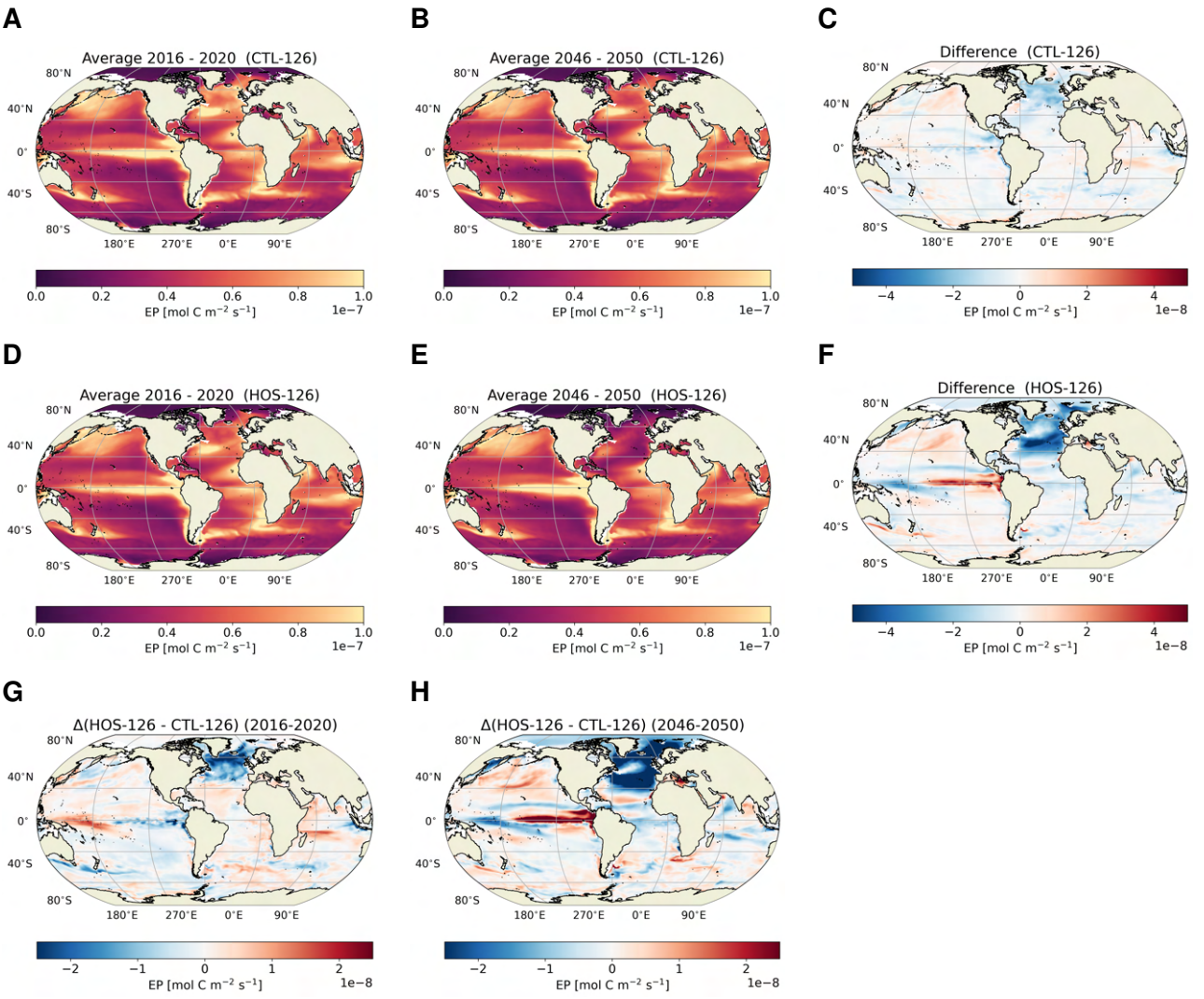

Figure 32. The Export Production (POC flux; EP) at 100 m depth in mol C m^{-2} s^{-1} for CTL-126 and HOS-126 and the difference between the two. The top row represents CTL-126 (A-C), the middle row HOS-126 (D-F), and the bottom row the difference (HOS-126 minus CTL-126; G, H). The left column represents the first decade (2015-2024; A, D, G), the middle column the last decade (2091-2100; B, E, H), and the right column the difference (last minus first; C, F).

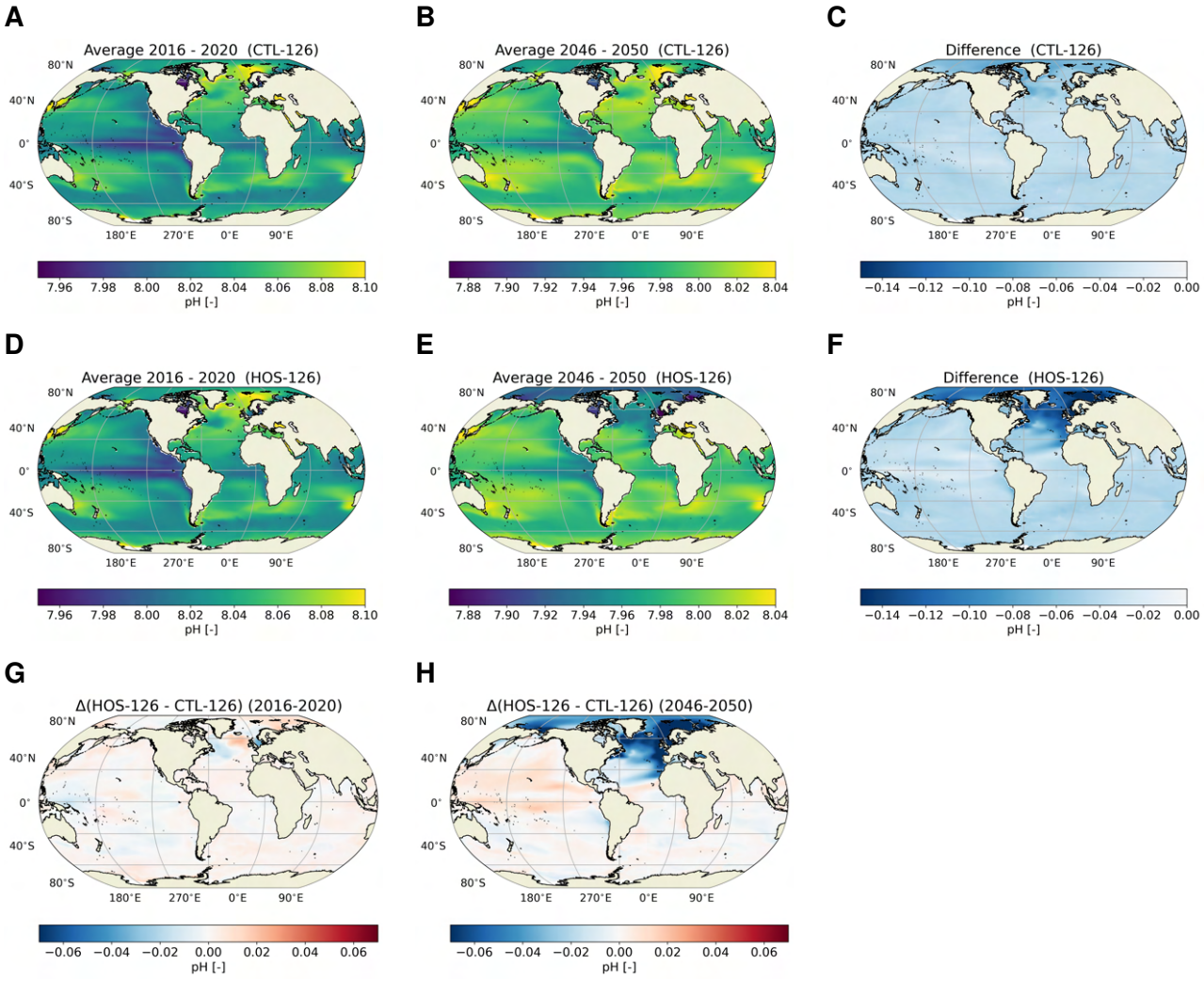

Figure 33. The pH of the surface ocean (unitless) for CTL-126 and HOS-126 and the difference between the two. The top row represents CTL-126 (A-C), the middle row HOS-126 (D-F), and the bottom row the difference (HOS-126 minus CTL-126; G, H). The left column represents the first decade (2015-2024; A, D, G), the middle column the last decade (2091-2100; B, E, H), and the right column the difference (last minus first; C, F).

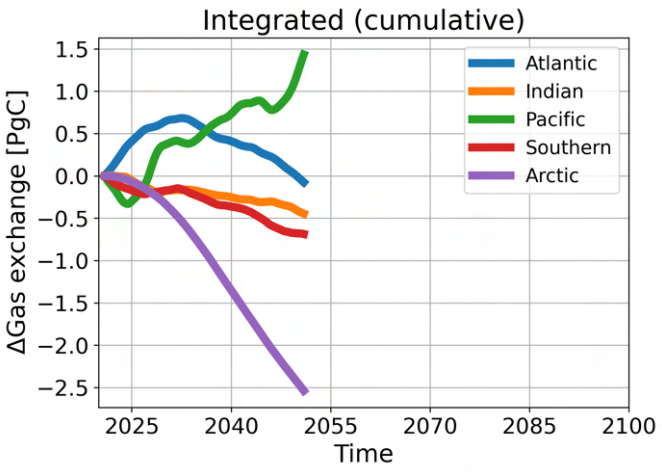

Figure 34. The difference between HOS-126 and CTL-126 for the exchange of CO_2 between the atmosphere and the ocean integrated over time and five different ocean basins in PgC: Atlantic Ocean (blue), Indian Ocean (orange), Pacific Ocean (green), Southern Ocean (red) and the Arctic Ocean (purple). The Southern Ocean is defined as the ocean south of 35°S, and the Arctic Ocean as the ocean north of 66°N.

References

Barker, S. and Knorr, G.: Millennial scale feedbacks determine the shape and rapidity of glacial termination, Nature Communications, 12, 2273, https://doi.org/10.1038/s41467-021-22388-6, https://doi.org/10.1038/s41467-021-22388-6, 2021.

Danabasoglu, G., Lamarque, J.-F., Bacmeister, J., Bailey, D. A., DuVivier, A. K., Edwards, J., Emmons, L. K., Fasullo, J., Garcia, R., Gettelman, A., Hannay, C., Holland, M. M., Large, W. G., Lauritzen, P. H., Lawrence, D. M., Lenaerts, J. T. M., Lindsay, K., Lipscomb, W. H., Mills, M. J., Neale, R., Oleson, K. W., Otto-Bliesner, B., Phillips, A. S., Sacks, W., Tilmes, S., van Kampenhout, L., Vertenstein, M., Bertini, A., Dennis, J., Deser, C., Fischer, C., Fox-Kemper, B., Kay, J. E., Kinnison, D., Kushner, P. J., Larson, V. E., Long, M. C., Mickelson, S., Moore, J. K., Nienhouse, E., Polvani, L., Rasch, P. J., and Strand, W. G.: The Community Earth System Model Version 2 (CESM2), Journal of Advances in Modeling Earth Systems, 12, e2019MS001 916, https://doi.org/https://doi.org/10.1029/2019MS001916, https://doi.org/10.1029/2019MS001916, 2020.

Dima, M. and Lohmann, G.: Evidence for Two Distinct Modes of Large-Scale Ocean Circulation Changes over the Last Century, Journal of Climate, 23, 5–16, https://doi.org/https://doi.org/10.1175/2009JCLI2867.1, https://journals.ametsoc.org/view/journals/clim/23/1/2009jcli2867.1.xml, 2010.

Eyring, V., Bony, S., Meehl, G. A., Senior, C. A., Stevens, B., Stouffer, R. J., and Taylor, K. E.: Overview of the Coupled Model Intercomparison Project Phase 6 (CMIP6) experimental design and organization, Geosci. Model Dev., 9, 1937–1958, https://doi.org/10.5194/gmd-9-1937-2016, https://gmd.copernicus.org/articles/9/1937/2016/https://gmd.copernicus.org/articles/9/1937/2016/gmd-9-1937-2016.pdf, 2016.

Jackson, L. C., Kahana, R., Graham, T., Ringer, M. A., Woollings, T., Mecking, J. V., and Wood, R. A.: Global and European climate impacts of a slowdown of the AMOC in a high resolution GCM, Climate Dynamics, 45, 3299–3316, https://doi.org/10.1007/s00382-015-2540-2, https://doi.org/10.1007/s00382-015-2540-2, 2015.

Liu, W., Duarte Cavalcante Pinto, D., Fedorov, A., and Zhu, J.: The Impacts of a Weakened Atlantic Meridional Overturning Circulation on ENSO in a Warmer Climate, Geophysical Research Letters, 50, e2023GL103 025, https://doi.org/https://doi.org/10.1029/2023GL103025, https://doi.org/10.1029/2023GL103025, 2023.

Long, M. C., Moore, J. K., Lindsay, K., Levy, M., Doney, S. C., Luo, J. Y., Krumhardt, K. M., Letscher, R. T., Grover, M., and Sylvester, Z. T.: Simulations With the Marine Biogeochemistry Library (MARBL), Journal of Advances in Modeling Earth Systems, 13, e2021MS002 647, https://doi.org/https://doi.org/10.1029/2021MS002647, https://doi.org/10.1029/2021MS002647, 2021.

Lynch-Stieglitz, J.: The Atlantic Meridional Overturning Circulation and Abrupt Climate Change, Annual Review of Marine Science, 9, 83–104, https://doi.org/10.1146/annurev-marine-010816-060415, https://doi.org/10.1146/annurev-marine-010816-060415, 2017.

Marchal, O., Stocker, T. F., and Joos, F.: Impact of oceanic reorganizations on the ocean carbon cycle and atmospheric carbon dioxide content, Paleoceanography, 13, 225–244, https://doi.org/https://doi.org/10.1029/98PA00726, https://doi.org/10.1029/98PA00726, 1998.

Matsumoto, K. and Yokoyama, Y.: Atmospheric Δ14C reduction in simulations of Atlantic overturning circulation shutdown, Global Biogeochemical Cycles, 27, 296–304, https://doi.org/https://doi.org/10.1002/gbc.20035, https://doi.org/10.1002/gbc.20035, 2013.

O'Neill, B. C., Carter, T. R., Ebi, K., Harrison, P. A., Kemp-Benedict, E., Kok, K., Kriegler, E., Preston, B. L., Riahi, K., Sillmann, J., van Ruijven, B. J., van Vuuren, D., Carlisle, D., Conde, C., Fuglestvedt, J., Green, C., Hasegawa, T., Leininger, J., Monteith, S., and Pichs-Madruga, R.: Achievements and needs for the climate change scenario framework, Nature Climate Change, 10, 1074–1084, https://doi.org/10.1038/s41558-020-00952-0, https://doi.org/10.1038/s41558-020-00952-0, 2020.

Palter, J. B.: The Role of the Gulf Stream in European Climate, Annual Review of Marine Science, 7, 113–137, https://doi.org/10.1146/annurev-marine-010814-015656, https://doi.org/10.1146/annurev-marine-010814-015656, 2015.

Rahmstorf, S.: Ocean circulation and climate during the past 120,000 years, Nature, 419, 207–214, https://doi.org/10.1038/nature01090, https://doi.org/10.1038/nature01090, 2002.

Schmittner, A. and Galbraith, E. D.: Glacial greenhouse-gas fluctuations controlled by ocean circulation changes, Nature, 456, 373–376, https://doi.org/10.1038/nature07531, https://doi.org/10.1038/nature07531, 2008.

Smith, R., Jones, P. W., Briegleb, P. A., Bryan, O., Danabasoglu, G., Dennis, M. L., Dukowicz, J. K., Eden, C., Fo Kemper, B., van Gent, R., Hecht, M., Jayne, S. R., Jochum, M., Large, G., Lindsay, K., Maltrud, M. E., Norton, J., Peacock, L., Vertenstein, M., and Yeager, S. G.: The Parallel Ocean Program (POP) reference manual: Ocean component of the Community Climate System Model (CCSM), 2010.

Vellinga, M. and Wood, R. A.: Global Climatic Impacts of a Collapse of the Atlantic Thermohaline Circulation, Climatic Change, 54, 251–267, https://doi.org/10.1023/A:1016168827653, https://doi.org/10.1023/A:1016168827653, 2002.

Vellinga, M. and Wood, R. A.: Impacts of thermohaline circulation shutdown in the twenty-first century, Climatic Change, 91, 43–63, https://doi.org/10.1007/s10584-006-9146-y, https://doi.org/10.1007/s10584-006-9146-y, 2008.

Weijer, W., Cheng, W., Drijfhout, S. S., Fedorov, A. V., Hu, A., Jackson, L. C., Liu, W., McDonagh, E. L., Mecking, J. V., and Zhang, J.: Stability of the Atlantic Meridional Overturning Circulation: A Review and Synthesis, Journal of Geophysical Research: Oceans, 124, 5336–5375, https://doi.org/https://doi.org/10.1029/2019JC015083, https://doi.org/10.1029/2019JC015083, 2019.

Weijer, W., Cheng, W., Garuba, O. A., Hu, A., and Nadiga, B. T.: CMIP6 Models Predict Significant 21st Century Decline of the Atlantic Meridional Overturning Circulation, Geophysical Research Letters, 47, e2019GL086 075, https://doi.org/https://doi.org/10.1029/2019GL086075, https://doi.org/10.1029/2019GL086075, 2020.